LBL-11541
Preprint

c.2

Lawrence Berkeley Laboratory
UNIVERSITY OF CALIFORNIA

ENERGY & ENVIRONMENT DIVISION

Submitted to Applied Optics

PHOTOTHERMAL DEFLECTION SPECTROSCOPY AND DETECTION

W. Jackson, Nabil M. Amer, A.C. Boccara, and D. Fournier

September 1980

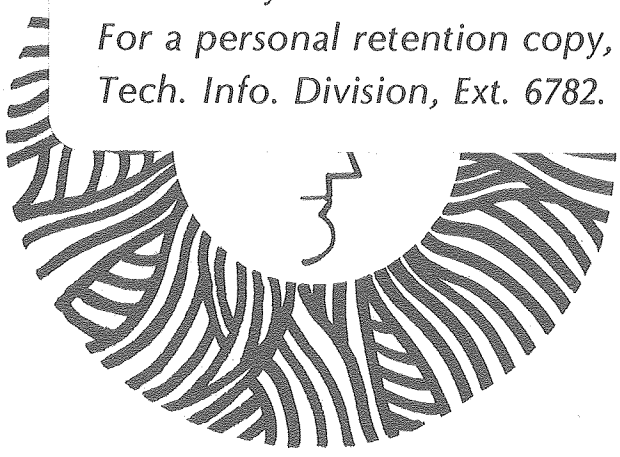

Prepared for the U.S. Department of Energy under Contract W-7405-ENG-48

DISCLAIMER

Photothermal Deflection Spectroscopy and Detection

W. Jackson and Nabil M. Amer

Applied Physics & Laser Spectroscopy Group

Lawrence Berkeley Laboratory

University of California

Berkeley, California 94720, USA

A. C. Boccara and D. Fournier

Laboratoire d'Optique Physique - E. R. 5 du CNRS

Ecole Superieure de Physique et de Chimie Industrielles

10, rue Vauquelin

75231 Paris Cedex 05, France

I. Introduction

It is well known that upon the absorption of electromagnetic radiation by a given medium, a fraction of or all of the excitation energy will be converted to thermal energy. In recent years, this de-excitation mechanism has provided the physical basis for a new class of sensitive photothermally based spectroscopies. Among the better known examples of these spectroscopies are interferometric techniques,[1] thermal lensing (TL),[2,3] photoacoustic spectroscopy(PAS),[4] and, most recently, photothermal deflection spectroscopy (PDS).[5-10] While the theoretical foundation of interferometry[1], TL[2,3] and PAS[11-16] are fairly well understood, this is not the case for PDS. Even though the concept of beam deflection by thermally induced changes in the index of refraction has been known for a long time,[17] to

Photothermal Deflection Spectroscopy and Detection

W. Jackson and Nabil M. Amer

Applied Physics & Laser Spectroscopy Group

Lawrence Berkeley Laboratory

University of California

Berkeley, California 94720, USA

A. C. Boccara and D. Fournier

Laboratoire d'Optique Physique - E. R. 5 du CNRS

Ecole Supérieure de Physique et de Chimie Industrielles

10, rue Vauquelin

75231 Paris Cedex 05, France

ABSTRACT

The theory for a sensitive spectroscopy based on the photothermal deflection of a laser beam is developed. We consider cw and pulsed cases of both transverse and collinear photothermal deflection spectroscopy for solids, liquids, gases, and thin films. The predictions of the theory are experimentally verified, its implications for imaging and microscopy are given, and the sources of noise are analyzed. The sensitivity and versatility of photothermal deflection spectroscopy are compared with thermal lensing and photoacoustic spectroscopy.

the best of our knowledge, no one has published a complete systematic theoretical or experimental investigation of the applicability of this phenomenon to spectroscopy. In this paper, we develop and experimentally verify a general theoretical treatment of PDS.

Before proceeding with the theoretical treatment of PDS, a brief physical description of PDS is in order. The absorption of the optically exciting beam (pump beam) causes a corresponding change in the index of refraction of the optically heated region. The absorption also causes an index-of-refraction gradient in a thin layer adjacent to the sample surface. By probing the gradient of the varying index of refraction with a second beam (probe beam), one can relate its deflection to the optical absorption of the sample. This is in contrast with probing thermally induced changes in optical path lengths, as in interferometric techniques or probing the curvature of the index of refraction as in TL. As can be seen from the above description, one has two choices in performing PDS: 1) collinear photothermal deflection[6,7,10] where the gradient of the index of refraction is both created and probed <u>within</u> the sample (Fig. 1) or 2) transverse photothermal deflection[5,8,9] where the probing of the gradient of the index of refraction is accomplished in the thin layer adjacent to the sample--an approach most suited for opaque samples and for materials of poor optical quality (Fig. 1). We have already demonstrated the high sensitivity of PDS for measuring <u>in situ</u> small absorptions in thin films, solids, liquids, and gases[5-8]. Its potential for imaging and scanning microscopy has been demonstrated[18].

In Sec. II, we present the theory of PDS for the cw collinear and transverse cases, and the pulsed collinear case. In Sec. III we deal with experimental considerations. The experimental results are compared with theoretical predictions in Sec. IV. Noise and background analysis are described in Sec. V, and in Sec. VI, we discuss our findings and compare them with related techniques. Finally, the implications of our calculations for imaging and microscopy are presented in Sec.

VII.

II. Theory

The calculation of the expected beam deflection for PDS can be divided into two parts. One first finds the temperature distribution in the sample and then solves for the optical beam propagation through an inhomogeneous medium. While temperature solutions have been reported in the literature[9,11-16], those reported are not applicable to our geometry and are not sufficiently general to provide a unified treatment for both collinear and transverse PDS of solids, thin films, gases, and liquids. We present a model which is sufficiently general to be applicable to most actual experimental cases.

A. Temperature Distribution

Consider the geometry shown in Fig. 1. Regions 0 and 2 are optically non-absorbing media. Region 1 is the absorbing medium, and can be either a thin film, gas, liquid, or solid. For simplicity, we assume that all three regions extend infinitely in the radial direction. This assumption does not significantly alter the applicability of the treatment since focussed laser beams are typically much smaller than the radial dimension of the sample, and the thermal diffusion length of most samples, is less than typical sample dimensions for experimentally useful chopping frequencies.

In the three regions, the temperature rise T, satisfies the equations,

$$\nabla^2 T_0 - \frac{1}{k_o}\frac{\partial T_o}{\partial t} = 0 \qquad \text{Region 0} \qquad (1a)$$

$$\nabla^2 T_1 - \frac{1}{k_1}\frac{\partial T_1}{\partial t} = \frac{-Q(\vec{r},t)}{\kappa_1} \qquad \text{Region 1} \qquad (1b)$$

$$\nabla^2 T_2 - \frac{1}{k_2}\frac{\partial T_2}{\partial t} = 0 \qquad \text{Region 2} \qquad (1c)$$

subject to the following boundary conditions

$$T_o\Big|_{z=0} = T_1\Big|_{z=0} \quad , \quad T_1\Big|_{z=\ell} = T_2\Big|_{z=\ell} \tag{2a}$$

and

$$\kappa_0 \frac{\partial T_o}{\partial z}\Big|_{z=0} = \kappa_1 \frac{\partial T_1}{\partial z}\Big|_{z=0} \quad , \quad \kappa_1 \frac{\partial T_1}{\partial z}\Big|_{z=\ell} = \kappa_2 \frac{\partial T_2}{\partial z}\Big|_{z=\ell} \tag{2b}$$

where κ_i is the conductivity, k_i ($k_i = \kappa_i / \rho_i C_i$) is the diffusivity, T_i is the temperature rise of the ith medium above the ambient temperature, and ℓ is the thickness of the absorbing medium. $Q(\vec{r},t)$ is the heat deposited per unit volume oscillating at the frequency ω in the absorbing medium and is given by

$$Q(\vec{r},t) = \frac{1}{2} \frac{4P\alpha}{\pi^2 a^2} e^{-\alpha z} e^{-2r^2/a^2} e^{i\omega t} + \text{c.c.} \tag{3}$$

for a square-wave intensity modulated beam where P is the optically exciting beam (pump beam) power, α is the absorption coefficient, and a is the $1/e^2$ radius of the Gaussian beam. We have assumed above that over the interaction region between the pump and probe beams, the probe beam is focussed to a smaller spot than that of the pump beam, and that the pump beam waist does not change over the confocal distance of the probe beam. In Eqs. (1a-c) we have also neglected the effect of the acoustic wave which accompanies the temperature rise of the illuminated volume. (See Appendix A for details).

Eqs. (1a-c) are solved by making the following substitutions. For region 0, we have

$$T_o(\vec{r},t) = \frac{1}{2} \int_0^\infty \delta d\delta J_o(\delta r)\, E(\delta)\, e^{\beta_o z} e^{i\omega t} + \text{c.c.} \quad ; \tag{4}$$

for region 2, we have

$$T_2(\vec{r},t) = \frac{1}{2}\int_0^\infty \delta d\delta J_o(\delta r)\, D(\delta)\, e^{-\beta_2(z-\ell)}\, e^{i\omega t} + c.c. \quad ; \tag{5}$$

and for region 1, we have

$$T_1(\vec{r},t) = \frac{1}{2}\int_0^\infty \delta d\delta J_o(\delta r)[\Gamma(\delta)\, e^{-\alpha z} + A(\delta)\, e^{-\beta_1 z} + B(\delta)\, e^{\beta_1 z}]\, e^{i\omega t} + c.c. \tag{6}$$

where $T_i(r,z)$ is the component of the temperature difference oscillating at frequency ω,

$$\Gamma(\delta) = \frac{P\alpha}{\pi^2 \kappa_1}\,\frac{e^{-(\delta a)^2/8}}{\beta_1^2 - \alpha^2} \quad , \tag{7}$$

and

$$\beta_i^2 = \delta^2 + i\omega/k_i \quad .$$

Substituting into Eqs. (1a-c) and satisfying the boundary conditions, we find that

$$\begin{aligned}
A(\delta) &= -[(1-g)(b-r)\, e^{-\alpha\ell} + (g+r)(1+b)\, e^{\beta_1\ell}]\, \Gamma(\delta)/H(\delta) \quad , \\
B(\delta) &= -[(1+g)(b-r)\, e^{-\alpha\ell} + (g+r)(1-b)\, e^{-\beta_1\ell}]\, \Gamma(\delta)/H(\delta) \quad , \\
D(\delta) &= \Gamma(\delta)\, e^{-\alpha\ell} + A(\delta)\, e^{-\beta_1\ell} + B(\delta)\, e^{\beta_1\ell} \quad , \\
E(\delta) &= \Gamma(\delta) + A(\delta) + B(\delta) \quad ,
\end{aligned} \tag{9}$$

and

$$H(\delta) = [(1+g)(1+b)\, e^{\beta_1\ell} - (1-g)(1-b)\, e^{-\beta_1\ell}]$$

where

$$g = \kappa_o\beta_o/\kappa_1\beta_1 \quad , \quad b = \kappa_2\beta_2/\kappa_1\beta_1 \quad , \quad r = \alpha/\beta_1$$

The final temperature distribution is obtained by combining Eqs. (4-9).

In order to gain insight into the physical picture discribed by the formulae and to relate our findings to previous work, we consider special cases.

To obtain the one dimensional solution[15], we take $2\pi \int_0^\infty rdr$ of Eq. (6). Since

$$\int_0^\infty \delta d\delta \int_0^\infty rdr\, J_o(\delta r)\, R(\delta) = R(0)$$

one obtains

$$\bar{T}_1(z) = 2\pi[\Gamma(0)\, e^{-\alpha z} + A(0)\, e^{-K_1 z} + B(0)\, e^{K_1 z}] \tag{10}$$

where

$$K_i^2 = i\omega/k_i \quad \text{and} \quad \bar{T}_1(z) = 2\pi \int_0^\infty rdrT_1(r,z) \quad .$$

Simplifying this expression, the result is

$$\begin{aligned}\bar{T}_1(z) = \frac{P\alpha}{H(0)\, \pi^2 \kappa_1 (K_1^2 - \alpha^2)} \; & [(1+g)(1+b)\, e^{K_1 \ell - \alpha z} \\ & - (1-g)(1-b)\, e^{K_1 \ell - \alpha z} - (1-g)(b-r)\, e^{-\alpha \ell - K_1 z} \\ & - (g+r)(1+b)\, e^{K_1(\ell - z)} - (1+g)(b-r)\, e^{-\alpha \ell + K_1 z} \\ & - (g+r)(1-b)\, e^{-K_1 \ell + K_1 z}\end{aligned} \tag{11}$$

Hence, the physical interpretation of Eqs. (4-6) is that any temperature distribution can be decomposed into distributions of the form $J_o(\delta r)e^{-\beta_i z}$. These distributions act independently of each other and have an effective thermal length given by

$$1_i = 1/\mathrm{Re}(\beta_i) = \{\mathrm{Re}[(K_i^2 + \delta^2)]^{1/2}\}^{-1}$$

The case $\delta=0$ gives a radially uniform temperature distribution which, as expected, is similar to the one dimensional case.

For region 1, $A(\delta)$ is the magnitude of the thermal wave diffusing in the positive z direction, $B(\delta)$ is the thermal wave diffusing in the negative z direction, and $\Gamma(\delta)$ is the temperature rise due to energy deposited at location (r,z) by the pump beam.

If heat diffusion into the bounding media is neglected and the temperature is integrated along the z direction, Eq. (6) reduces to

$$\int_0^{\ell} dz\, T_1(\vec{r},t) = \frac{1}{2}\,\frac{P(1 - e^{-\alpha\ell})}{\pi^2 K_1}\int_0^{\infty}\frac{\delta J_o(\delta r)\, e^{-(\delta a)^2/8}}{\delta^2 + K_1^2}\, d\delta e^{i\omega t} + c.c. \qquad (12)$$

If the thermal length $(\mathrm{Re}K_1)^{-1}$, is much smaller than the beam radius, the denominator in Eq. 12 becomes K_1^2 and the integral can be performed. The result is[6]

$$\int_0^{\ell} dz\, T_1(\vec{r},t) = \frac{1}{2}\,\frac{P(1 - e^{-\alpha\ell})4}{\pi^2 i\omega(\rho C)_1 a^2}\, e^{-2r^2/a^2}\, e^{i\omega t} + c.c. \qquad (13)$$

In the above case, the temperature distribution follows the beam profile because there is no diffusion of heat.

If the thermal length is much greater than the beam radius, K_1^2 can be neglected in the denominator of Eq. 12. The solution for the temperature gradient reduces to[6]

$$\int_0^{\ell} dz\, T_1(\vec{r},t) = \frac{1}{2}\,\frac{P(1 - e^{-\alpha\ell})}{\pi^2 K_1 r}\,[1 - e^{-2r^2/a^2}]\, e^{i\omega t} + c.c. \qquad (14)$$

This result shows that the temperature distribution extends significantly beyond the beam profile for low chopping frequencies.

B. Optical Beam Propagation

We next calculate the effect of the temperature distribution on the

probe beam. The index of refraction is, in general, a function of temperature and pressure. One can neglect the pressure contribution (see Appendix A). Hence,

$$n(\vec{r},t) = n_o + \Delta n(\vec{r},t)$$

$$= n_o + \left.\frac{\partial n}{\partial T}\right|_{T\ \text{ambient}} T(\vec{r},t) \tag{15}$$

where $\frac{\partial n}{\partial T}$ is typically $10^{-4}\ {}^{o}C^{-1}$ for liquids and $10^{-5}\ {}^{o}C^{-1}$ for solids. The propagation of the Gaussian probe beam through the spatially varying index of refraction is given by[19]

$$\frac{d}{ds}\left(n_o \frac{d\vec{r}_o}{ds}\right) = \vec{\nabla}_\perp\ n(\vec{r},t) \tag{16}$$

where $\vec{r}_o$ is the perpendicular displacement of the beam from its original direction, n_o is the uniform index of refraction, and $\nabla_\perp\ n(r,t)$ is the gradient of the index of refraction perpendicular to $\vec{S}$ (the ray path) (see Fig. 2). The change in the complex beam parameter, q, is given by[19]

$$\frac{d}{ds}\left(1/q_{S_{i\perp}}\right) = -\left(\frac{1}{q_{S_{i\perp}}}\right)^2 - \frac{\partial^2 n}{n_o \partial S_{i\perp}^2} \qquad i = 1,2 \tag{17}$$

where

$$1/q_{S_{i\perp}} = 1/R_{S_{i\perp}} - i\lambda/(n_o \pi w_o^2)$$

$R_{S_{i\perp}}$ is the radius of curvature of the phase fronts, w_o is the $1/e^2$ spot size, and λ is the vacum wavelength of the probe beam. We also assume that the deflection is small compared to the temperature distribution. Since typical deflections are 10^{-5} radians over 1 cm, the total deviation is 0.1 μm, which is much smaller than the typical 50 μm spot size of a focussed laser. Integrating Eqs. (16) and (17) over the ray path $\vec{S}$ gives

$$\frac{d\vec{r}_o}{ds} = \frac{1}{n_o}\int_{\text{path}} \vec{\nabla}_\perp\ n(\vec{r},t)ds \tag{18}$$

and

$$1/q_{S_{i\perp}}\Big|_{\substack{\text{end of}\\ \text{interaction}}} - 1/q_{S_{i\perp}}\Big|_{\substack{\text{Beginning of}\\ \text{interaction}}} = \int_{\text{Path}} ds\left(-\frac{1}{q_{S_{i\perp}}^2} - \frac{\partial^2 n}{n_o \partial S_{i\perp}^2}\right) \quad i=1,2 \quad (19)$$

Since the deviation is small,

$$\frac{d\vec{r}_o}{ds} \cong \phi = \frac{1}{n_o}\frac{\partial n}{\partial T}\int_{\text{Path}} \vec{\nabla}_\perp T(\vec{r},t)\, ds \quad (20)$$

where ϕ is the angular deviation from $\vec{S}$ and Eq. (15) was used. Eq. (20) is a three-dimensional generalization valid for Gaussian beams of the one dimensional case reported in Ref. 8. From Eq. (19) we see that the effect of the curvature of the index of refraction is equivalent to an astigmatic lens of focal length, F_i, in the S_i direction where F_i is given by

$$1/F_i = -\frac{1}{n_o}\int_{\text{Path}} \frac{\partial^2 n}{\partial S_{i\perp}^2}\, ds = -\frac{1}{n_o}\frac{\partial n}{\partial T}\int_{\text{Path}} \frac{\partial^2 T}{\partial S_{i\perp}^2}\, ds \qquad i = 1,2 \quad (21)$$

Eqs. (20) and (21) demonstrate one of the differences between PDS and TL. PDS probes the gradient of the temperature while TL probes its curvature.

C. Solution for Beam Deflection

1. Collinear PDS

For collinear PDS, the beam is deflected by the temperature gradient in all three regions. For simplicity, we assume that the probe beam travels parallel to the pump beam axis and is deflected only in Regions 1 and 2.[20] However, the interaction length is restricted to be consistant with an angle between the pump and probe beams (see Fig. 3).

From Eqs. (5), (6), and (18), the deflection in this case is given by

$$\phi = \frac{-e^{i\omega t}}{2n_o}\frac{\partial n}{\partial T}\left[\int_0^{\ell} dz \int_0^{\infty} \delta^2 d\delta J_1(\delta x_o)\, \Gamma(\delta)\, e^{-\alpha z} + A(\delta)\, e^{-\beta_1 z} + B(\delta)\, e^{\beta_1 z}\right.$$
$$\left. + \int_0^{\ell_i} dz \int_0^{\infty} \delta^2 J_1(\delta x_o)\, d\delta D(\delta)\, e^{-\beta_2(z-\ell)}\right] + \text{c.c.} \qquad \ell_i > \ell \quad (22)$$

where $\ell_i = 2a/\sin\psi$ is the length of interaction of the two beams, x_o is the displacement between the beams, and ψ is the angle of their intersection. If the beams overlap in Region 1 only, then

$$\phi = -\frac{1}{2n_o}\frac{\partial n}{\partial T} e^{i\omega t} \int_0^{\ell_i} dz \int_0^{\infty} \delta^2 d\delta J_1(\delta x_o)[\Gamma(\delta)\, e^{-\alpha z} + A(\delta)\, e^{-\beta_1 z} + B(\delta)\, e^{\beta_1 z}] + c.c. \qquad \ell_i < \ell \tag{23}$$

Note that the assumption that the beams are parallel can be relaxed by integrating over an oblique path and evaluating the gradient in a perpendicular direction. This would add unnecessary complexity without introducing any significant effects.

2. Transverse PDS

For transverse PDS, the probe beam propagates completely within Region 0. The probe beam path is (see Fig. 1)

$$y = y_o \qquad z = (\tan\psi)x + z_o \tag{24}$$

For small tan ψ, $\nabla_\perp T = \frac{\partial T}{\partial z}$. By substituting Eq. (4) into Eq. (20), the deflection is given by

$$\phi = \frac{1}{2}\frac{e^{i\omega t}}{n_o}\frac{\partial n}{\partial T}\int_{-\infty}^{-z_o/(\tan\psi)} dx \int_0^{\infty} \delta J_o(\delta\sqrt{y_o^2 + x^2})\, \beta_o E(\delta)\, e^{[(\tan\psi)x + z_o]\beta_o} + c.c. \tag{25}$$

3. Pulsed PDS

For pulsed PDS, the temperature solution as a function of time can be found by replacing $i\omega$ by p in Eqs. (22)-(25) and inverting the Laplace transform using the inversion formula

$$\phi(t) = \frac{1}{2\pi i}\int_{c-i\infty}^{c+i\infty} \phi(p)\, e^{pt}\, dt \tag{26}$$

Because of the integral form of the solution and the many poles of the integrand, this solution would be too cumbersome to be of use. For an

infinite, weakly absorbing medium, the solution is much simpler and is qualitatively similar to the more complicated solution. Hence, we derive this solution for a square pulse.

In this case, the temperature is given by[21]

$$T(r,t) = \int_0^t dt'' \int_0^\infty 2\pi r' dr' Q(r',t'')\, G(r',r,t-t'') \tag{27}$$

where

$$Q(r',t'') = \begin{cases} \dfrac{2\alpha E_o}{\pi a^2 t_o} e^{-2r'^2/a^2} & 0 \le t'' \le t_o \\ 0 & t'' > t_o \end{cases},$$

$$G(r',r,t-t'') = \frac{1}{4\pi\kappa_1 (t-t'')} \exp\left[\frac{-(r^2 + r'^2)}{4k_1(t - t'')}\right] I_o\left(\frac{rr'}{2k_1(t - t'')}\right)$$

E_o is the pulse energy, and t_o is the pulse width.

Integrating and solving for $\partial T/\partial r$, we obtain

$$\frac{\partial T}{\partial r} = \frac{-\alpha E_o}{\pi \kappa_1 t_o 2r}\left[e^{-2r^2/(a^2+8k_1 t)} - e^{-2r^2/a^2}\right] \qquad 0 \le t \le t_o \tag{28}$$

$$\frac{\partial T}{\partial r} = \frac{-\alpha E_o}{\pi \kappa_1 t_o 2r}\left[e^{-2r^2/(a^2+8k_1 t)} - e^{-2r^2/(a^2+8k_1 (t-t_o))}\right] \qquad t > t_o$$

This expression may be substituted into Eq. (20) (and letting r=a/2) to derive the expected signal versus time at the position of maximum deflection.

D. Numerical Evaluation

Eqs. (22) and (23) were evaluated using numerical quadrature routines. By varying the method of integration and the step size, and by comparing the results with limiting cases and experiments, we verified

that the routines were converging correctly. The equations were evaluated using appropriate material parameters and the results of the calculations are shown in Figs. 6-13 and will be compared with the experimental results.

III. Experimental Considerations

A. Experimental Configurations

Experiments were performed to verify the theoretical results and to determine the ultimate sensitivity of PDS[5-8]. The experimental configurations are given in Fig. 4. Fig. 4a shows the experimental set-up for transverse PDS. For exciting light sources (pump beams), we used either a cw dye laser, a pulsed dye laser, or a xenon arc lamp with a monochromator. When a cw dye laser or an arc lamp was used, a mechanical chopper modulated the output. The probe beam was a 0.5 mW HeNe laser. Two types of position sensors[22] were used to determine the amplitude and phase of the probe beam deflection: lateral and quadrant. The output of the sensor was fed into the (A-B) input of a lockin amplifier.

In Fig. 4b, the experimental arrangement for collinear PDS is presented. The pump beam must be a laser in order to permit tight focussing. To minimize the scattering of the pump beam on the position sensor, both pump and probe beams were counter propagating. Furthermore, a notch filter was placed between the sample and the detector to eliminate any remaining scattered light. To maximize the signal, the angle between the pump and probe beams can be minimized, although collinearity is rarely required. One further consideration is that the

focal spot of the probe beam should be smaller than that of the pump beam.

In the case of pulsed PDS, the exciting light source was a Chromatix CMX-4 flashlamp-pumped dye laser. A quadrant position sensor detected the deflection of the HeNe probe beam. The output of the sensor was fed into a differential preamplifier whose output was digitized by a Tektronix 7912AD digitizer. When necessary, this digitized waveform was averaged with a Tektronix 4052 computer. The laser power was monitored with a color corrected photodiode for the purpose of power normalization.

Sample materials included filtered spectroscopic grade benzene, a 0.5 μm thick film of indium and tin oxides deposited on a glass substrate, and a 600 nm glass edge filter.

B. Analysis of Detector Response

As indicated above, the deflection of the beam due to the change in the index of refraction is detected by a position sensor which converts the deflection into an output voltage. The relationship between the deflection and the voltage depends on whether the position sensor is a quadrant or a lateral detector.

For a quadrant detector, the change of the signal V above the DC level, V, is calculated using Fig. 5a. Assuming a Gaussian probe beam,

$$\frac{\Delta V}{V} = \frac{\Delta I}{I_o} = 4\ \Delta x \int_o^\infty \frac{2}{\pi w_2^2} e^{-2r^2/w_2^2} dr$$

$$= (4/\sqrt{2\pi})\ \frac{\Delta x}{w_2} \qquad (29)$$

where $\Delta x = \phi d$, d is the distance from the focal spot to the detector, I_o is the probe beam intensity, and w_2 is the spot radius on the detector. Since d is large,

$$w_2 \cong \frac{\lambda d}{\pi w_o n_o} \tag{30}$$

where w_o is the probe beam radius at the focal spot. Hence,

$$\Delta V = \frac{4}{\sqrt{2\pi}} \frac{\phi \pi w_o n_o}{\lambda} V \tag{31}$$

and ϕ is given by Eq. (20).

We conclude that in the case of a quadrant position sensor, the signal is independent of the sample distance. For modulation frequencies of the order of a few hundred cycles per second, $\Delta V/V$ was found to be 10^{-6}. Thus, we were able to measure a deflection of 1.5×10^{-9} radian/$\sqrt{\text{Hz}}$ given typical laser parameters.

For a lateral detector, we use the sensitivity figure of 0.55P amps/cm given by the manufacturer where P is the probe beam power in watts. Then, $\Delta V/V = 0.55\Delta x = 0.55\phi d$ (d is in cm). The signal depends on the distance from the focal spot to the detector. For a detector of size ℓ_1 (see Fig. 5b),

$$d_{max} = \frac{\ell_1 \pi w_o n_o}{\lambda} \tag{32}$$

so

$$\frac{\Delta V}{V} = \frac{0.55\phi}{2} \frac{\ell_1 \pi w_o n_o}{\lambda} \tag{33}$$

Since $\ell_1 = 1$ cm, we see that both detectors are similar in sensitivity.

IV. Experimental Verification of the Theoretical Predictions

A. CW PDS

As noted above, PDS can be performed in two ways: collinear and transverse. Experiments were conducted to evaluate both approaches and to compare the results obtained with the theoretical predictions.

1. Collinear PDS

a. Signal Dependence on Intra-beam Offset (x_o)

Fig. 6a shows the dependence of the signal amplitude on the offset of the pump and probe beams for high and low modulation frequencies. Note that both theoretical curves are adjusted only by the identical amplitude factor, indicating that the correct relative magnitude and peak positions are predicted by the theory.

The discrepancy in the case of high modulation frequency and larger x_o could be due to uncertainty in the precise thermal properties of the glass substrate. Similarly, the phase shown in Fig. 6b demonstrates good agreement between theory and experiment, except for large displacements[23].

For low frequencies, the thermal lengths in the sample and the substrate are much larger than the pump beam radius. Consequently, the temperature distribution extends significantly beyond the beam radius. Fig. 6b shows that the phase changes continuously as the probe beam moves away from the pump beam. This is due to the propagation of the heat from the pump beam to the probe beam. For high frequencies, the thermal conduction becomes unimportant. Hence, the curve describing the relationship between the amplitude and the offset of the pump and probe

beams is the radial derivative of the beam profile. Using this fact, one can measure the radius of the Gaussian beam profile, if unknown, and check the focus of the pump beam. Far from the pump beam, the phase changes linearly with the distance, x_o, since it is due to the propagation delay of the heat wave traveling from the pump to the probe beam.

b. Signal Dependence on Modulation Frequency (ω)

Figs. 7a and 7b show the amplitude and phase versus the frequency for various offsets of the probe beam. The theoretical amplitude is adjusted by an amplitude factor, and the phase is adjusted with a constant offset. The theoretical and experimental curves show rapid change at the same frequency and approach the same limiting values at high frequencies. When the thermal length in the sample-substrate becomes smaller than the probe beam radius, the signal amplitude and the phase change rapidly. Thus, by measuring the pump beam radius, using the technique outlined above, one can measure the thermal diffusivity of the sample. The high frequency limit of the signal amplitude has a $1/\omega$ dependence. When the probe beam is offset from the pump beam by more than one beam radius, the signal decreases faster than $1/\omega$. This occurs not only because the temperature of the central region decreases as $1/\omega$, but because the thermal length also decreases, preventing the heat from reaching the probe beam. If the two beams overlap significantly, there is no dependence on the thermal length. This causes the high frequency limit to follow $1/\omega$.

2. Transverse PDS

For the transverse PDS, several parameters were varied.

a. Frequency Dependence

By examining Fig. 8 we see that the signal falls off very rapidly as a function of frequency. Because $T \propto \exp(z_o/l_t)$, the signal falls off exponentially as the frequency increases. The important consequence of the above is that for high modulation frequencies, pulsed work, or solids immersed in liquids, the signal is bigger if the probe beam is carefully aligned closely to the sample surface and, hence, should be focussed. This condition shows that the signal is optimized for flat samples with small lateral dimensions.

b. Signal Dependence on Pump Beam Radius (a)

Fig. 9 shows the effect of varying the pump beam radius. The signal increases as 1/a as the pump beam is focussed. The temperature rise has an a^2 dependence, while the interaction length goes as 1/a. When the pump beam radius becomes as small as the lateral thermal length, no further increase in the signal is observed. For z_o less than the thermal length in air (l_a), the lateral thermal length is approximately the thermal length in the glass (l_g); for z_o greater than l_a, the lateral thermal length is approximately l_a.

c. Signal Dependence on Probe and Pump Beam Offset (y_o)

Fig. 10 shows the effect of off-axis displacement (y_o) of the probe beam relative to the pump beam (see Fig. 1). By varying the offset (y_o) of the beams, the profile of the temperature in region 0 is probed at

the position z_o of the probe beam. The main peak width is determined by the spot size of the pump beam and the sample thermal length. Because l_a is larger than l_g, the heat flows from the air back into the sample for y_o greater than l_g (see inset in Fig. 10). This reversed heat flow causes the second, but weaker, maximum, with its phase shifted 180^o from that of the central peak. For z_o greater than l_a, the heat flows away from the sample for all y_o values, and the secondary peak will no longer be observed.

d. Signal Dependence on the Probe Beam Tilt Angle (ψ)

The effect of varying the tilt angle, ψ, of the probe beam relative to the sample surface is shown in Fig. 11. For a small pump radius (40 μm), the tilt angle is not important unless the sample actually intercepts the probe beam. In the case of a broad band pump beam (0.71 cm), the signal is more sensitive to the tilt angle because of the longer path grazing the sample. This often requires a longer focal length lens for the probe beam.

e. Pump Beam Offset In the z_o Direction

Fig. 12 shows the effects of varying the beam offset (z_o) from the sample. In general, the signal increases exponentially as the probe beam approaches the sample. As pointed out in Ref. 5, the exponential increase can be used to determine the diffusivity of the deflecting medium. For the more realistic case of a beam focussed on a poor conducting substrate, the results are more complex. For z_o increasing, the temperature distribution is determined by the thermal properties of the air (or an appropriate fluid) so the beam deflection falls off exponentially as l_a. On the

other hand, for z_o decreasing, the temperature distribution gets smaller and more compressed (see Fig. 10). Hence, the signal rises faster than exponentially.

Spectra taken with cw PDS have been previously reported and will not be repeated here[5-8]. For transverse PDS and for an interaction length of 1 cm, we were able to detect a temperature rise of 10^{-4} °C in air and 10^{-6} °C for CCl_4. For collinear PDS, we have been able to measure an $\alpha\ell$ of 10^{-8} for liquids[6], 10^{-7} for solids[6], and 10^{-7} for gases[7].

B. Pulsed Collinear PDS

We have investigated the case of collinear pulsed PDS. The signal as a function of time for pure benzene is shown in Fig. 13. The measured time constant(1/e) is 6.2 ms. The magnitude of the expected signal was computed using Eq. (28) with r = a/2 = 37 μm. The pump radius (a) was found by measuring the distance the pump beam focussing lens moved between signal maxima. The agreement between theory and experiment is good, demonstrating that for thick uniform samples, the finite sample approximation is appropriate.

To demonstrate the sensitivity of pulsed PDS, we have obtained the spectrum of the sixth harmonic of the C-H stretch of 0.1% of benzene in distilled CCl_4 (Fig. 14a). The measured absorption coefficient is 2×10^{-6} cm^{-1}. Since the interaction length was 0.1 cm or less, we measured an $\alpha\ell$ of 10^{-7}. We believe the background is due to impurities in the CCl_4 (since such a background was 10 times larger before distillation of CCl_4), absorption in the CCl_4 itself, or is due to the signal caused by electrorestriction[24].

Fig. 14b shows the signal versus time for the peak absorbtion in 0.1% benzene. The rise time is determined by the shunt capacitance of the cables with a 50 kΩ load resistor. The fall time is determined by a 5000 Hz high pass filter in the preamplifier. The signal-to-noise ratio for a single point can be conservatively estimated to be 10. (Actually, if one were to fit a curve through all points, the noise would be considerably less.) Assuming a signal-to-noise ratio of 10, we find that we can measure an absorption coefficient of 2×10^{-7} cm^{-1} for 1 mJ laser. Since the noise appears to be mostly shot noise, the HeNe probe laser output could be increased by a factor of 20, giving an improvement of 4 in the S/N ratio. If one fits a curve through all points and takes more averages, the minimum measureable absorption coefficient can be lowered by a factor of 10-100. This assumes that problems with coherent electrical noise, electrorestriction, and probe laser noise are insignificant.

V. Noise - Background Considerations

The background noise originates from the following sources: laser noise (pointing and intensity fluctuations), electronic noise, and sample and/or ambient environment noise (e.g. convection, turbulence, or mechanical vibration).

For cw PDS, the pointing noise of the probe laser predominates. The intensity fluctuations of the probe beam can be discriminated against by adjustment of the probe spot on the detector. Typically, the differential input can reject intensity fluctuations to 1 part in 1000. For a typical laser, the ratio of the intensity noise to the DC level was $5 \times 10^{-6}/\sqrt{Hz}$, while the observed noise ratio was $6 \times 10^{-7}/\sqrt{Hz}$. The expected contribution of laser intensity fluctuations is $5 \times 10^{-9}/\sqrt{Hz}$

which is much less than the observed noise. Also, the observed noise can not be attributed to room vibrations or air turbulence since the noise decreased by a factor of 10 when we used a focussed flashlight beam as the probe beam. We conclude that the noise must be due to pointing fluctuations. Testing a variety of HeNe lasers, we found that they all exhibited a pointing noise of roughly 5×10^{-9} radians/$\sqrt{\text{Hz}}$ at low frequencies reaching shot noise at a few kHz. Spatial filtering or installation of an intra cavity iris could improve this value.

The electronic noise is easily calculated and seldom limits the sensitivity. Following Van der Ziel's analysis[24], the expected combined rms current noise contribution of the position sensor, the load resistor, and the preamplifier is given by

$$i_{RMS} = (4k_B T F_1)^{1/2} \left(\frac{1}{R_L} + \frac{eI_o}{2k_B T} + \frac{i_n^2}{4k_B T} + \frac{e_n^2}{4R_L^2 k_B T} + \frac{e_n^2 \omega^2 C'^2}{12\, k_B T} \right)^{1/2} \qquad (34)$$

where k_B is Boltzman's constant, T is the temperature, F_1 is the frequency band pass of the detector and electronics, R_L is the load resistor, I_o is the d.c. current, C' is the combined detector, cable, and preamplifier shunt capacitance, i_n is the preamplifier current noise, and e_n is the preamplifier voltage noise. Usually, the third term in Eq. (34) can be neglected for a reasonably good amplifier by making the load resistor larger than 1KΩ. Often the first and fourth terms can be neglected as well. This is feasible at low frequencies. Thus, the most significant electronic noise term is the shot noise, the second term, which sets a detection limit of 3.4×10^{-10} rad/$\sqrt{\text{Hz}}$ for a 1 mW probe laser.

For wide band or pulsed operation, the situation is more complicated. The high frequency cutoff, F_1 is determined by $2\pi F_1 R_L C'=1$. Consequently, the load resistance cannot be made arbitrarily large. Furthermore, since the thermal signal fall time is very slow (see Fig. 13), the high pass filter must be set at 25 Hz or less to avoid waveform distortion. Unfortunately, a 25 Hz high pass filter allows significant low frequency noise and background into the detection electronics. We have found that a 3000 Hz high pass filter improves the signal-to-noise ratio and eliminates the background significantly, even though it distorts the waveform and throws away part of the signal. The distorted waveform is shown in Fig. 14b. With a high pass filter, the shot noise predominates over other noise sources.

Other factors which may contribute to the background noise are unwanted light scattered on the position sensor, spurious signals due to particulates, impurities in the sample, and window absorption. In the case of low modulation frequencies in liquids, turbulence may mask the true deflection of the probe beam. Obvious solutions to these problems include keeping thermal gradients small, filtering out particles, distilling the liquid, and insuring that the probe and pump beams do not overlap within the windows of the sample container.

VI. Discussion and Comparison with Related Spectroscopies

In this section we discuss the advantages and disadvantages of PDS, and compare PDS to other photothermally-based spectroscopies. A summary of our comparision is given in Table I.

A. Comparisons to Thermal Lensing (TL)

First, we compare collinear PDS to TL given in Ref. 3 . Using the recommendations found therein, we determine that for weak absorptions, the relative change of intensity $\Delta I/I$ for TL is given by

$$(\Delta I/I)_{TL} = 0.8 \frac{w_o^2}{\lambda} \frac{\partial n}{\partial t} \frac{\alpha P \ell_{TL}}{a^2 \kappa_1} \left[\frac{1}{1 + t_c/2t}\right] \tag{35}$$

where w_o is the probe focal spot, a is the pump focal spot, t is the time after pump is turned on, α is the absorption coefficient, P is the pump beam power, ℓ_{TL} is the interaction length, κ_1 is the conductivity, λ is the vacum wavelength of the probe beam, n_o is the index of refraction of the media, and $t_c = a^2/4k$. Using Eq. (29) for the change of intensity $\Delta I/I$ for PDS and evaluating $\partial T/\partial r$ as in Ref. 3, we find that

$$(\Delta I/I)_{PDS} = \frac{4\alpha P}{\sqrt{2\pi}} \frac{w_o}{\lambda} \frac{\partial n}{\partial T} \frac{\ell_{PDS}}{a\kappa_1} (e^{-1/2(1+2t/t_c)} - e^{-1/2}) \tag{36}$$

letting $t \to \infty$ and assuming $n_o = 1.5$

$$\frac{(\Delta I/I)_{PDS}}{(\Delta I/I)_{TL}} = \frac{0.78\ \ell_{PDS}}{\ell_{TL}} \tag{37}$$

If the probe beam is aligned collinearly with the pump beam and if the pump is filtered out before reaching the position sensor, then the following relation holds:

$$\ell_{PDS} = \ell_{TL} = 0.2\ \pi w_o^2 n_o / \lambda \tag{38}$$

Thus PDS and TL have almost the same sensitivity. Usually, however, for

both collinear PDS and TL, the overlap of the beams within the notch filter can give rise to an appreciable background signal due to heating within the filter. To reduce the background, the pump and probe beams should intersect at an angle. This reduces the interaction length and the signal by a factor of one to two orders of magnitude.

PDS has several distinct advantages over TL when one considers noise and background. The probe laser usually has relatively large intensity fluctuations. Such fluctuations give rise to significant noise in the case of TL, but are reduced in PDS by a factor of 1000. The pointing noise of the probe laser, of course, affects both PDS and TL. When PDS and TL are used on semiconductors with a bandgap near the probe wavelength, the probe beam intensity will be modulated by the shift of the band gap due to pump beam heating. This intensity modulation causes an additional signal which varies as the pump wavelength. The two contributions may be difficult to separate.

PDS also has versatility advantages over TL. Spectra of opaque samples or scattering samples can be measured using transverse PDS, 3-dimensional depth profiling of absorption can be performed by moving the beam overlap region through the sample. Finally, TL is more difficult to align. Hence, PDS is as sensitive as TL and is more versatile and easy to use.

B. Comparison with Photoacoustic Spectroscopy (PAS)

Because of the variety of detector-sample combinations of both PAS and PDS, we will restrict our comparison to condensed matter samples.

Compared with microphone PAS, PDS has the following advantages: 1)

PDS is more sensitive, particularly in the case of liquids, 2) PDS has the potential for remote sensing and *in situ* monitoring, 3) PDS works in hostile environments such as temperature extremes or caustic substances, 4) acoustic shielding requirements are less stringent, 5) there is no backgound due to window absorption, 6) the frequency response is greater, 7) spatial probing of absorption is possible, and 8) the complication of gas coupling physics is eliminated. The disadvantages of PDS are: 1) alignment is more difficult, 2) the sample surface can not be exceedingly rough, and 3) for collinear PDS, the sample must be transparent to the probe beam for collinear PDS.

Compared with piezoelectric PAS, the advantages of PDS are: 1) PDS is at least as sensitive, 2) PDS can be employed in hostile environments, 3) there is no scattering background, 4) the attachment of the transducer to the sample is eliminated, 5) the mechanical properties and sample size are not limiting factors, 6) 3-dimensional spatial profiling is possible, and 7) the relationships of the signal to the temperature rise and to the time dependence of the signal are far simpler. On the other hand, the disadvantages of PDS are: 1) in the case of collinear PDS it may be difficult to find a probe beam that is transmitted by some materials, 2) alignment is more difficult, and 3) the optical quality of the sample is more demanding for collinear PDS.

VII. Implications for Imaging and Microscopy

Recently, photoacoustic detection, which depends on both the optical and the thermal properties of a given material, has been put to use in performing scanned imaging and microscopy of various materials.[26-28] In this case, a new type of image is obtained which displays unique spatial and thermal information. Of particular interest is the ability of

this imaging to detect subsurface structures or flaws which exist at depths exceeding the optical penetration of the probe light.

The discussion presented above suggests that photothermal deflection detection yields information similar to photoacoustic imaging. Photothermal deflection imaging has been reported elsewhere.[18] In this section we discuss some of the implications of our theoretical treatment for imaging and microscopy.

A. Collinear Photothermal Deflection Microscopy and Imaging

This scheme is mainly suitable for optically thin samples and for weakly absorbing objects imbeded in a transparent matrix. By scanning the interaction region of the focussed pump and probe beams relative to the sample, a three dimensional profile can be constructed. In this case, the optical resolution is determined by the size of the probe beam waist in the x and y directions, and by the interaction length ℓ_i ($=2a/\sin\psi$) in the z direction. Consequently, the larger the intersection angle of the beams and the tighter the focal spot of the pump beam, the greater the optical resolution. On the other hand, we have shown that the thermal resolution is determined by the thermal length within the sample itself (see Eq. 12 and Fig. 6a). Fig. 6a shows that as the modulation frequency increases, the thermal resolution given by $(\mathrm{Re}\ K_1)^{-1}$ also increases.

We have demonstrated[6] that an $\alpha\ell$ of 10^{-7} can be measured with collinear PDS. Hence, spatial profiling of weakly absorbing inhomogeneities can be probed with a resolution equal to the pump laser spot size. By changing the probe wavelength, one can get spectral information as well.

B. Transverse Photothermal Deflection Microscopy and Imaging

By performing transverse photothermal deflection microscopy, one probes the optical and thermal properties at and near the surface of the material of interest. The optical resolution will again be determined by the pump beam waist , while the thermal resolution for a focussed pump beam will be the thermal wavelength in the material. For large pump beams or for large thermal sources, the thermal resolution is more complicated. In the case of small beam offsets ($|z_o|$), the thermal resolution is given by the thermal length in the sample. For large $|z_o|$, however, the thermal resolution is given by the thermal wavelength in deflecting media adjacent to the sample surface.

Transverse photothermal deflection microscopy also can yield information on the surface topography of a given material. Eq. (25) and Fig. (12) show the strong dependence of the signal on the probe beam offset ($|z_o|$). If the material's surface varies in the z direction, both the phase and the amplitude of the photothermal deflection signal will reflect such a variation.[18] In the case of a uniformally illuminated surface with a uniform absorption, surface roughness of the order of 0.1μm can be resolved.

To account fully for the role of sample inhomogeneities and of geometrical boundaries and to determine the thermal resolution, one needs to genralize our theoretical treatment to include the spatial variation of the thermal properties of the sample. Such an extension will not be dealt with in this paper.

VIII. Summary

We have shown that photothermal deflection spectroscopy is a sensi-

tive and versatile techique for measuring a wide range of absorption coefficients in solids, thin films, liquids, and gases. A model was presented which accurately predicts the experimental results. The model allows the experimenter to optimize the experimental setup and quantitatively predict the sensitivity and limitations of PDS. We also identifed sources of noise and ways to maximize the signal-to-noise ratios were discussed. Finally, we discussed the advantages and disadvantages of PDS and compare it to alternative spectroscopies. We believe that photothermal deflection spectroscopy will prove to be a unique and sensitive spectroscopic technique.

We express our sincere thanks to C. B. Moore, members of his group, and A. Kung for the generous use of a Chromatix CMX-4 laser. We also thank the other members of the Applied Physics and Laser Spectroscopy Group and M. Jackson for their helpful suggestions and comments. This work was supported by the U. S. Department of Energy under Contract W-7405-ENG-48.

Appendix A

The acoustic wave deflects the probe beam in two ways. The acoustic wave propagates for the energy deposition region to the probe beam where it generates a temperature rise by adiabatic compression. The gradient of this temperature rise deflects the beam. The ratio of this term to the thermal deflection term is

$$(\text{Acoustic/Thermal}) = (k_o B^2 \omega T_o / C\rho) \exp(z_o / \ell_t)$$

where B_T is the volume expansion coefficient, $l_t = (2k_o/\omega)^{\frac{1}{2}}$ and z_o is the distance between the heat deposition region and the probe beam. This ratio is the same as the ratio given in Ref. 9. For gases and liquids

$$\frac{\text{Acoustic}}{\text{Thermal}} \cong 10^{-11}\ \omega e^{z_o/\ell_t}$$

which indicates that the acoustic term will be important only at very high frequencies and/or large probe displacements between the heat deposition region and the probe beam. When the acoustic and thermal contributions to the deflection are equal, the signal will be 10^{-10} times smaller than the thermal deflection signal for low frequencies and z=0. Hence, the acoustic terms add considerable complexity, but are negligble in most practical experiments.

The acoustic wave also deflects the probe beam by the pressure generated at the sample surface. The pressure wave propagates to the probe beam and deflects the probe beam through the pressure dependence of the index of refraction. The contribution of the pressure deflection term is of the same order of magnitude as the contribution in Eq. (A1) if a gas is the deflecting medium. For liquids, it is negligble. Ref. 9 leaves this term out. Hence, to be consistant one must solve the coupled pressure and temperature waves in the sample and deflecting medium, and compute their combined effect on the index of refraction. The additional terms will be of nominal experimental importance only at high frequencies, large probe beam offsets, and/or high pump beam peak powers.

References

1. See, for example, J. Stone, J. Opt. Soc. Am., 62, 327 (1972); J. Stone, Appl. Opt. 12, 1828 (1973).

2 J. R. Whinnery, Acc. of Chem. Res. 7, 225 (1974) and references therein.

3. R. L. Swofford and J. A. Morrell, J. Appl. Phys. 49, 3667 (1978) and references therein.

4 For an overview of photoacoustic spectroscopy see Y.-H. Pao, ed., Optoacoustic Spectroscopy and Detection, (Academic Press: New York 1977).

5. D. Fournier, A. C. Boccara and J. Badoz, presented at the Topical Meeting on Photoacoustic Spectroscopy, Iowa State University, Ames, Iowa, Aug. 1-3, 1979.

6. A. C. Boccara, D. Fournier, W. Jackson, and N. M. Amer, Opt. Lett., 5, 377 (1980).

7. D. Fournier, A. C. Boccara, N. M. Amer, and R. Gerlach, Appl. Phys. Lett., 37, 519 (1980).

8. A. C. Boccara, D. Fournier, and J. Badoz, Appl. Phys. Lett, 36, 130 (1980).

9. J. C. Murphy and L. C. Aamodt, J. Appl. Phys. (Sept. 1980).

10. M. Billardon and J. M. Ortega, (private communication).

11 F. A. McDonald and G. C. Wetsel, Jr., J. Appl. Phys. 49, 2313 (1978).

12. W. Jackson and N. M. Amer, J. Appl. Phys. 51, 3343 (1980).

13 H. S. Bennett and R. A. Forman, J. Appl. Phys. 48, 1432 (1977).

14. L. C. Aamodt and J. C. Murphy, J. Appl. Phys 49, 3036 (1978).

15 A. Rosencwaig and A. Gersho, J. Appl. Phys. 47, 64 (1976).

16 A. Mandalis and B. S. Royce, J. Appl. Phys., 50, 4331 (1979).

17. D. C. Smith, IEEE J. Quant. Elec., QE-5, 600 (1969).

18 D. F. Fournier and A. C. Boccara in Scanned Image Microscopy, E. A. Ash, Ed., (London: Academic Press, 1980).

19. L. W. Casperson, Appl. Opt., 12, 2434 (1973).

20 For some high frequency modulation experiments with very tight focussing, we observed a small secondary maximum with a 180° phase shift. Because the pump and probe beams intersect at an angle and the probe beam deflects slightly in Region 0, a mechanism, similar to that discussed in Sec. IV.A.2(c), could be present.

21. H. S. Carslaw and J. C. Jaeger, Conduction of Heat in Solids, (Oxford: Claredon Press, 1959).

22. Silicon Detector Corporation, Newbury Park, California.

23. In some cases, it is experimentally advantageous to use a liquid in Region 0 to make use of the typically higher dn/dt for liquids. In this case, it is obvious that the role of Region 0 and Region 2 should be interchanged.

24. S. R. Brueck, H. Kildal, and L. J. Belanger, Opt. Comm., 34, 199 (1980).

25. A. Van der Ziel, Noise in Measurements (Wiley, New York, 1976).

26 R. L. Thomas, J. J. Pouch, Y. H. Wong, L. D. Favro P. K. Kuo, and A. Rosencwaig, J. Appl. Phys. 51, 1152 (1980), and references therein.

27 H. K. Wickramasinghe, R. C. Bray , V. Jipson, C. F. Quate, and J. R. Salcedo, Appl. Phys. Lett. 33, 923 (1978).

28 G. Busse and A. Ograbeck, J. Appl. Phys. 51, 3576 (1980), and references therein.

TABLE I.
SUMMARY OF SOME THERMALLY BASED SPECTROSCOPIES

Technique	Samples Already Studied	Experimental Set Up	Sensitivity $(\alpha\ell)_{min}$ x Pump Power (W)[a]	Probe Beam	Sensitivity to Scattered Light	Special Features
TL	Liquids	Difficult to align	10^{-7} -10^{-8}	Sensitivity to pointing and intensity noise	No	No mechanical contact. Permits hostile environment and in situ measurements.
Microphone PAS	Solids (bulk, powder), liquids, & gases	Simple to align	$\sim 10^{-4}$ - 10^{-5} solids 10^{-7} gasses		Yes	Sensitive to mechanical and accoustical noise.
PZT PAS	Solids (bulk) liquids	Simple to align	$\sim 10^{-5}$ (10^{-9} J pulsed)		Yes	Sample attachment difficult.
Collinear PDS	Optically clean transparent solids, liquids & gases	Difficult to align	$\sim 10^{-7}$ -10^{-8} (10^{-10} J pulsed)	Sensitivity to pointing noise Sample transparent to probe	No	No mechanical contact. Permits hostile environment and in situ measurements.
Transverse PDS	Condensed phase samples	Simple to align	$\sim 10^{-5}$	Sensitivity to pointing noise	No	No mechanical contact. Permits hostile environment and in situ measurements.
Interferometry	Liquids & solids	Difficult to align	$\sim 10^{-7}$ -10^{-8}	Sensitive to intensity noise Sample transparent to probe beam	No	No mechanical contact. Permits hostile environment and in situ measurements.

[a]Typical ranges cited in the literature.

Figure Captions

Fig. 1. Geometry for theory. The heat deposited diffuses into region 0 and region 2 as well as radially. For transverse PDS, the probe beam axis maybe displaced along the y axis by a distance y_o.

Fig. 2. Scattering geometry. The scattering region may focus the beam differently in the $S_{1\parallel}$ and $S_{2\perp}$ directions (elliptical Gaussian beams).

Fig. 3. Effective interaction length in collinear PDS. For simplicity, beams are assumed to be parallel but interact only over a distance ℓ_i.

Fig. 4. Experimental apparatus. (a) Transverse PDS. (b) Collinear PDS.

Fig. 5. (a) Probe spot on detector. (b) Continuous detector. Maximum distance from probe focal spot to the detector is d_{max}.

Fig. 6. Collinear PDS. (a) Signal amplitude vs. beam displacement x_o/a. (b) Signal phase vs. beam displacement x_o/a.

Fig. 7. Collinear PDS. (a) Signal amplitude vs. frequency. (b) Signal phase vs. frequency.

Fig. 8. Transverse PDS. Signal vs. frequency for various offsets (z_o). The beam radius is 140 μm.

Fig. 9. Transverse PDS. Signal amplitude vs. beam radius (a) for different beam offsets (z_o). The frequency is 48 Hz and the tilt angle is 0^o.

Fig. 10. Transverse PDS. Signal amplitude vs off-axis displacement (y_o) for various z_o offsets. The material is 600 nm edge filter glass, the frequency is 48 Hz, the tilt angle is 0^o, and the beam radius is 70 μ m. Inset shows the direction of heat flow and the origin of the second maximum.

Fig. 11. Transverse PDS. Signal amplitude vs. tilt angle (ψ). The frequency is 48 Hz, and the sample is 600nm edge filter glass.

Fig. 12. Transverse PDS. Signal amplitude vs. beam offset (y_o) at 48 Hz. The tilt angle is 0^o.

Fig. 13. Signal vs. time for benzene at 607 nm. Collinear PDS with the probe beam at x_o=a/2.

Fig. 14. (a) Absorption vs. wavelength for 0.1% benzene in distilled CCl_4. (b) Signal vs. Time. The horizontal scale is 1 ms/div, the wavelength is 606 nm , and 1024 averages were taken.

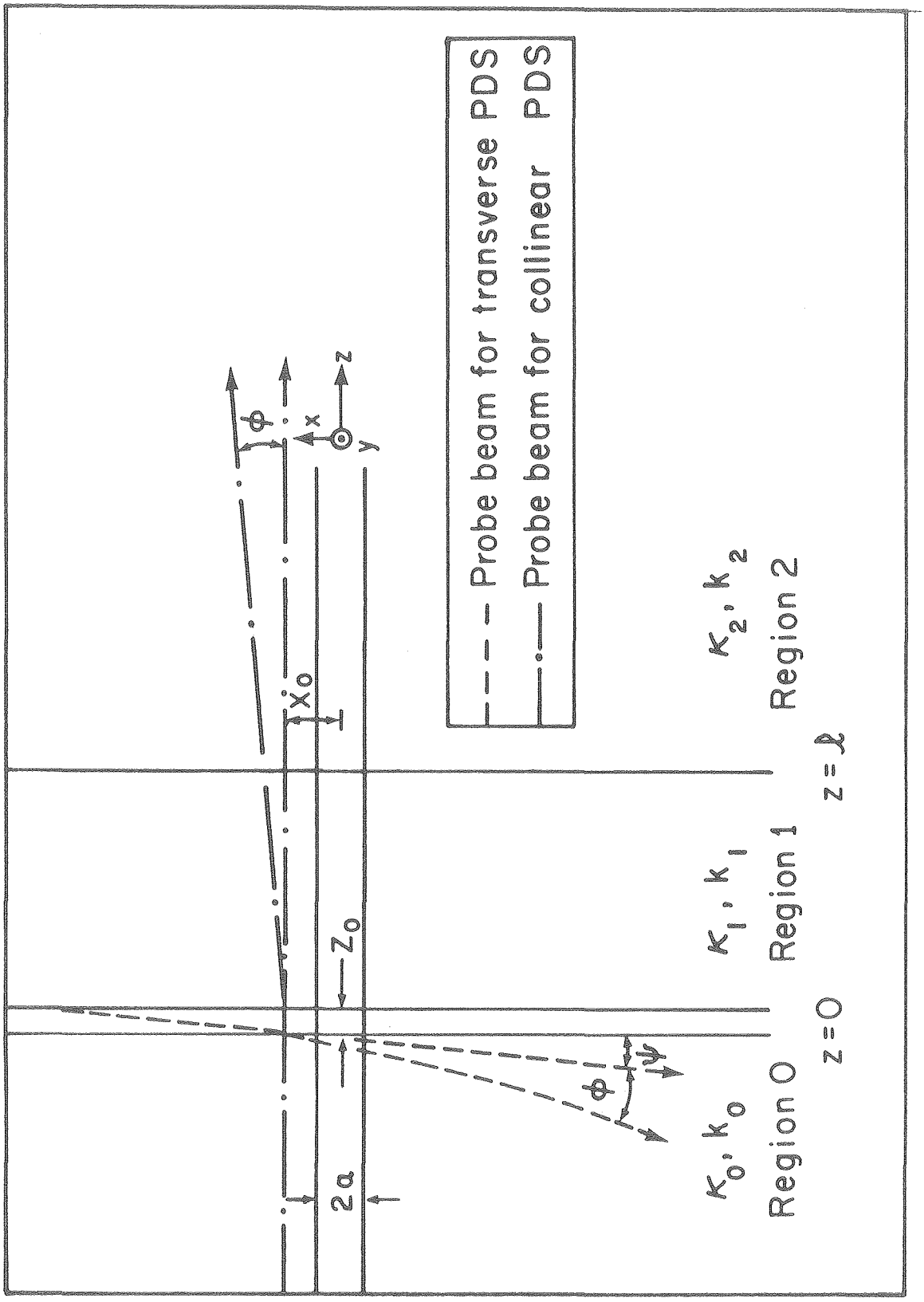

XBL8010-2089

Fig. 1

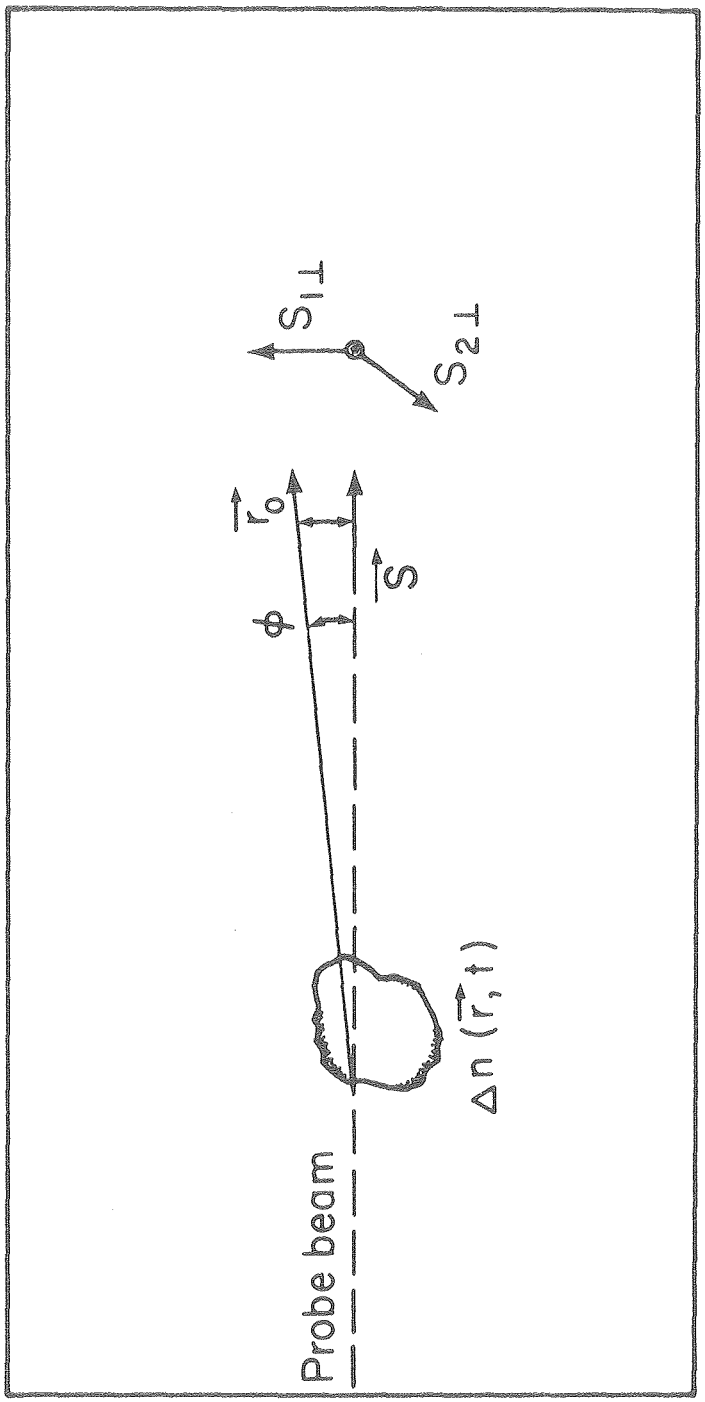

XBL8010-2088

Fig. 2

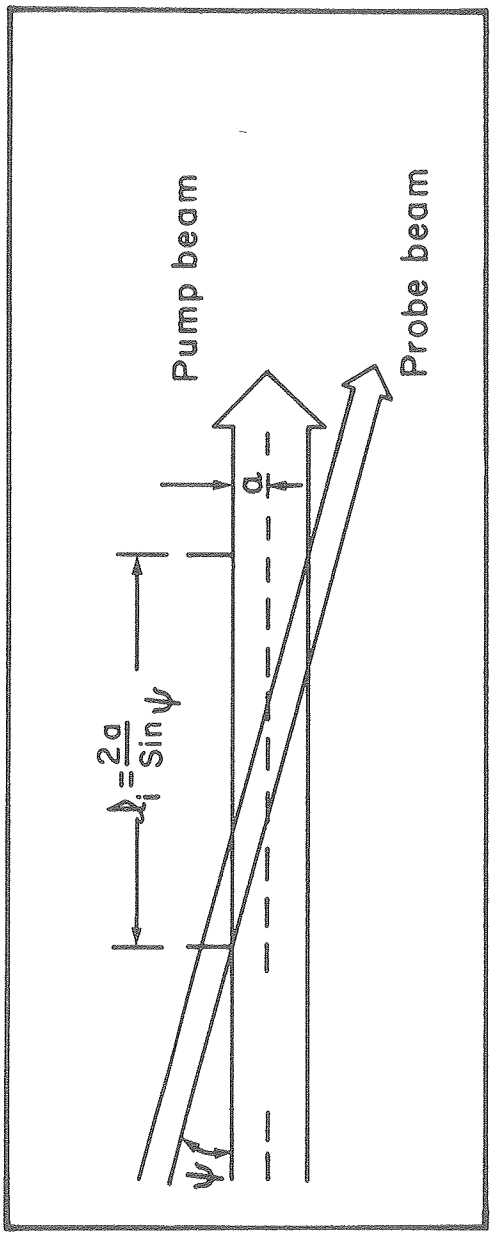

XBL 8010-2083

Fig. 3

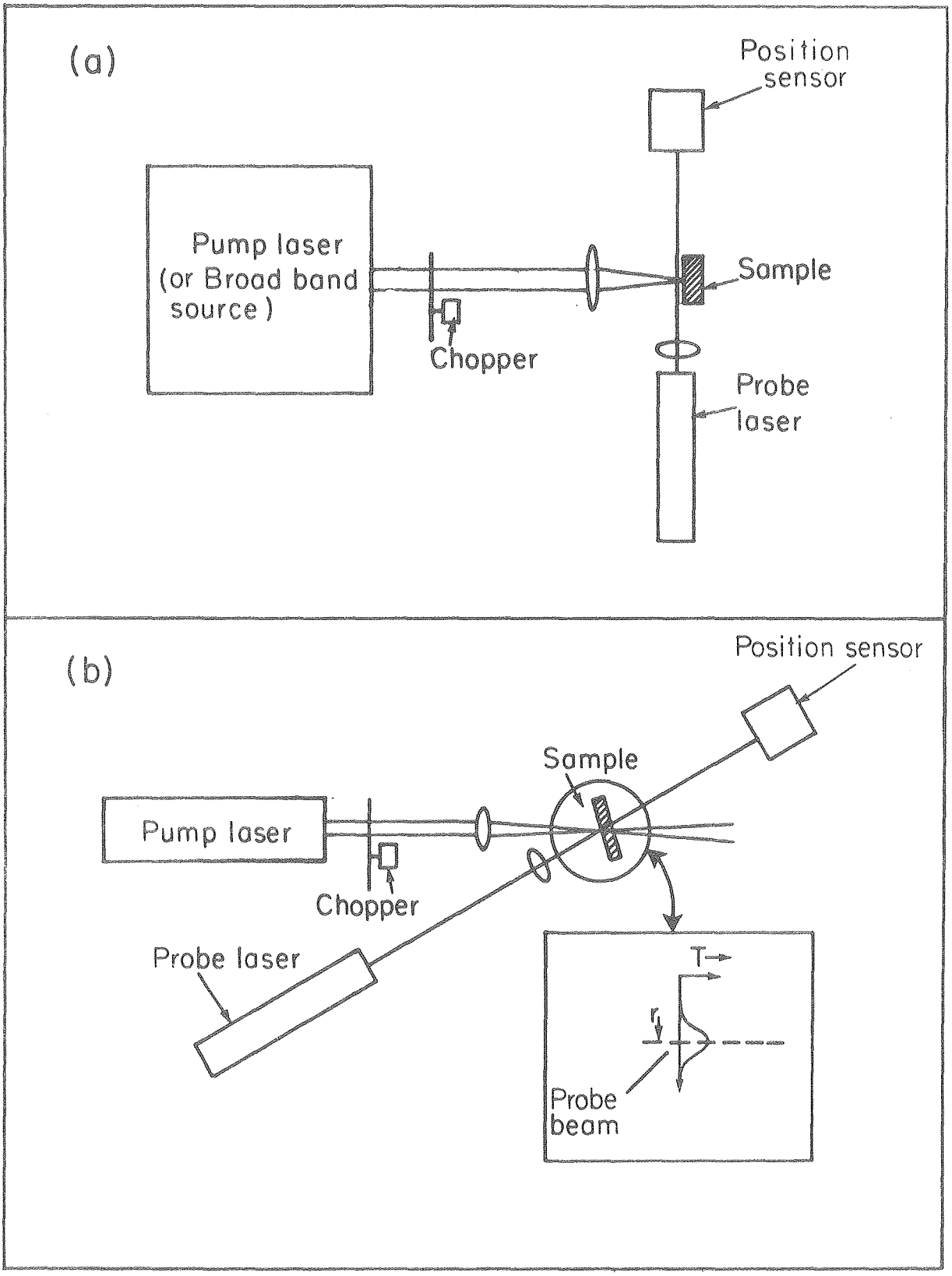

Fig. 4

XBL8010-2073

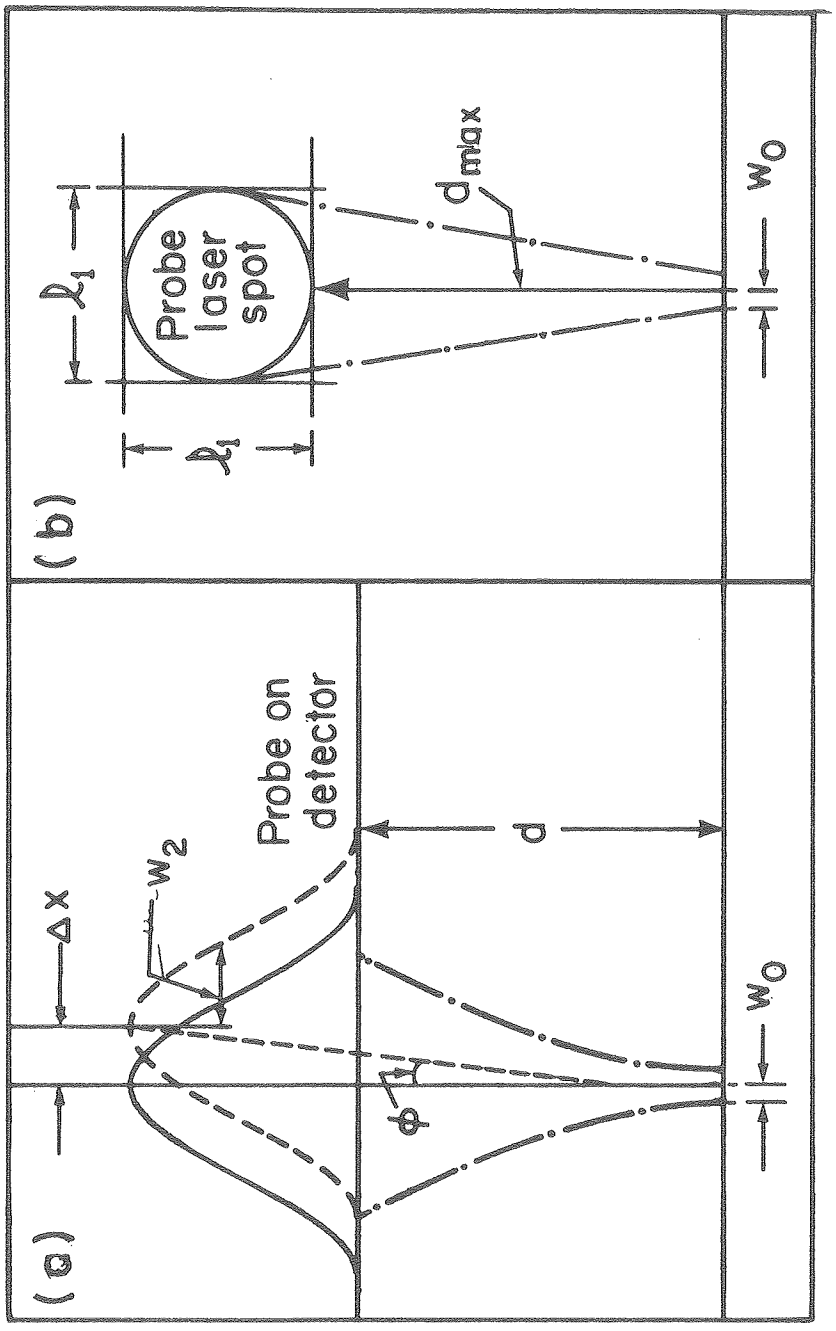

XBL8010-2082

Fig. 5

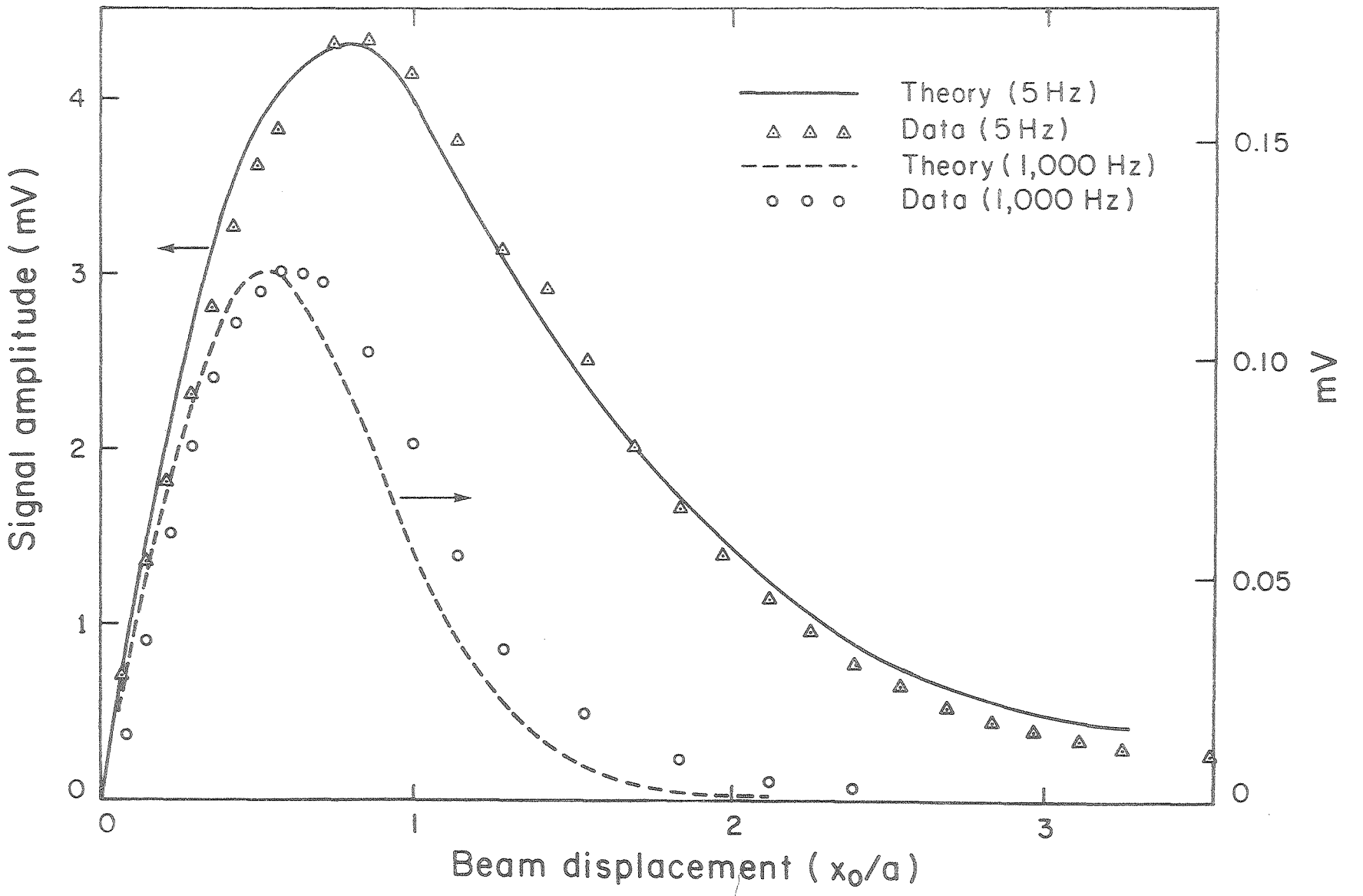

XBL 8010-2080

Fig. 6a

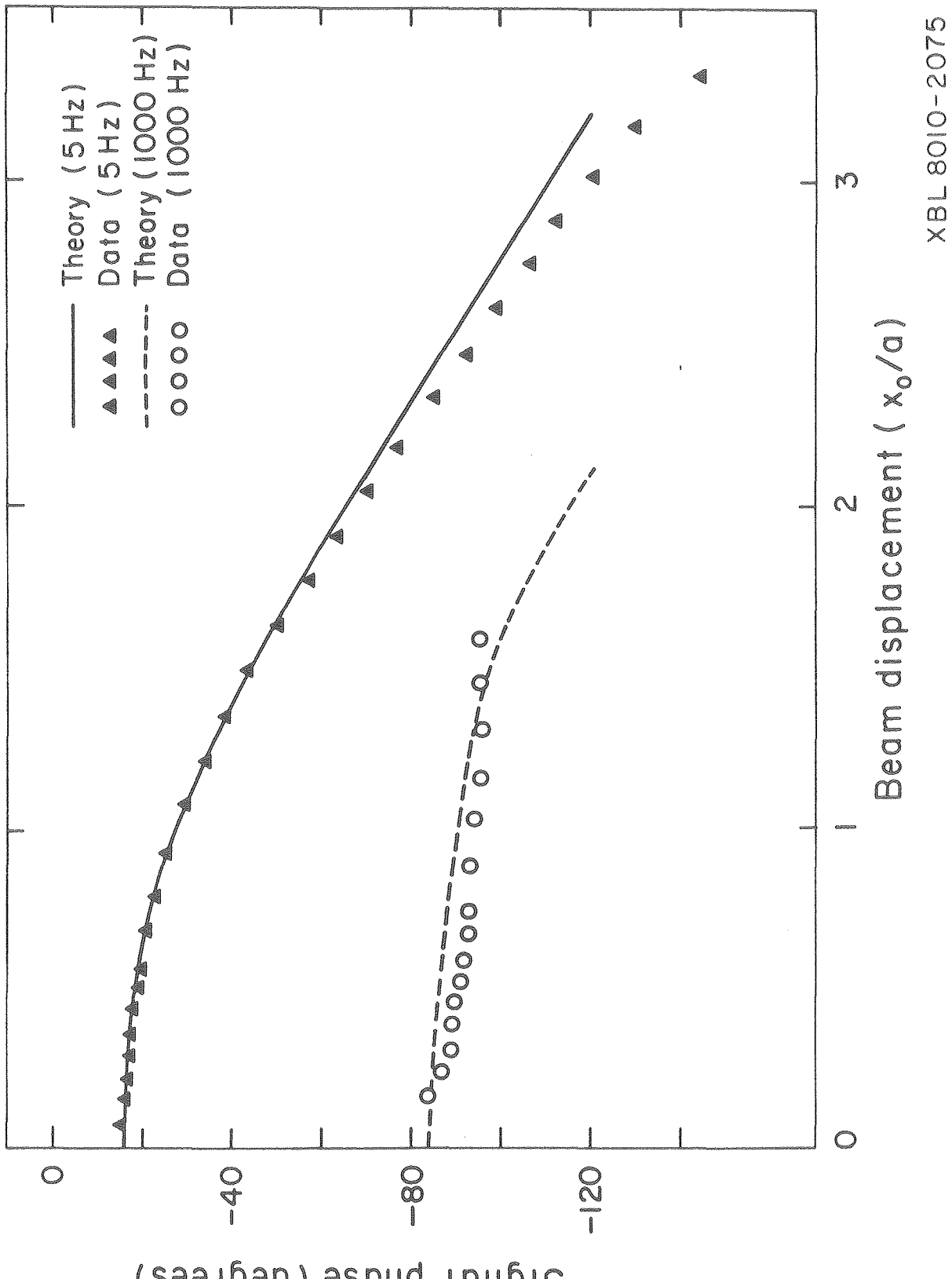
Theory (5 Hz)
Data (5 Hz)
Theory (1000 Hz)
Data (1000 Hz)
Signal phase (degrees)
0
-40
-80
-120
0
1
2
3
Beam displacement (x_o/a)
XBL 8010-2075

Fig. 6b

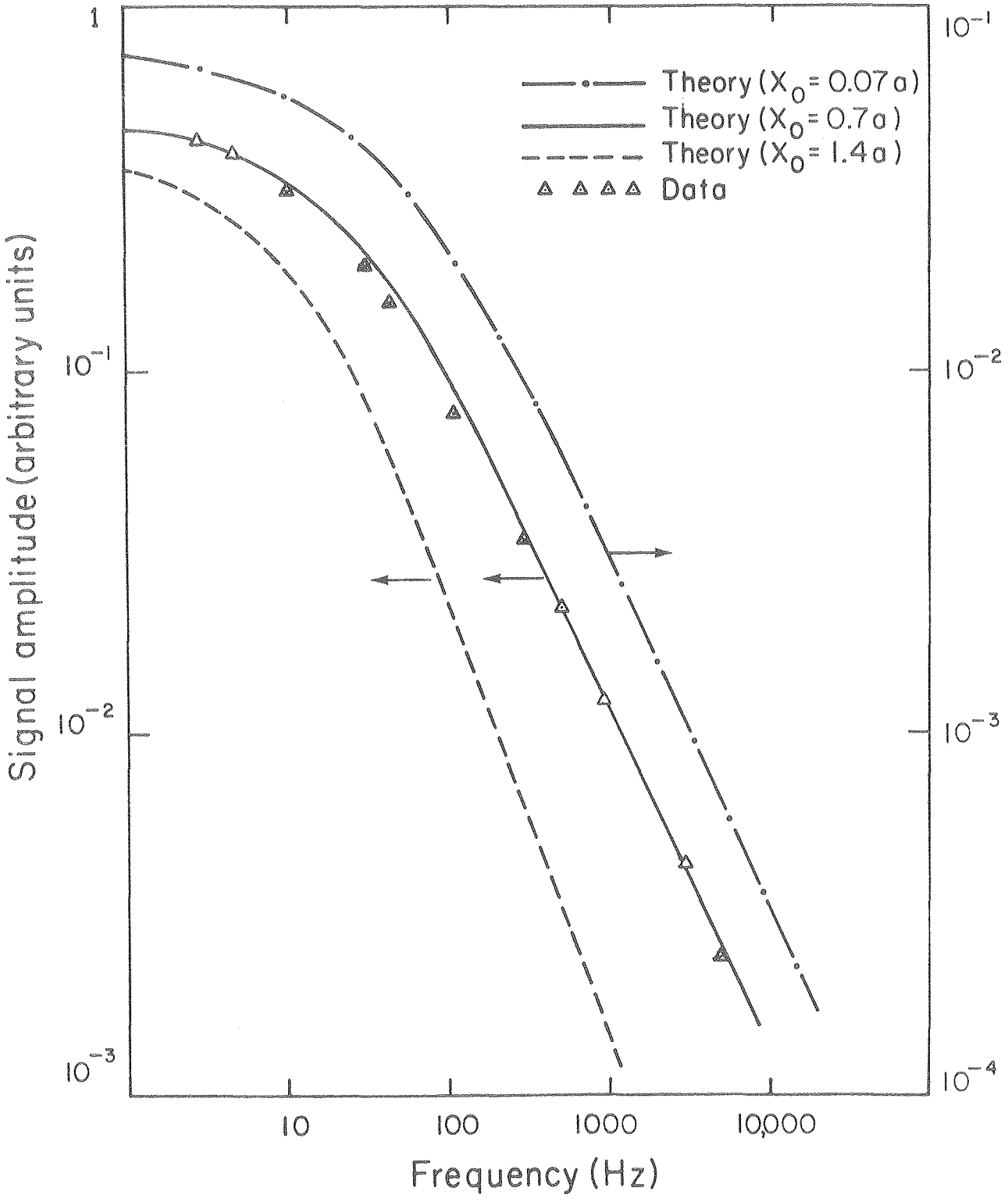

Fig. 7a

XBL 8010-2078

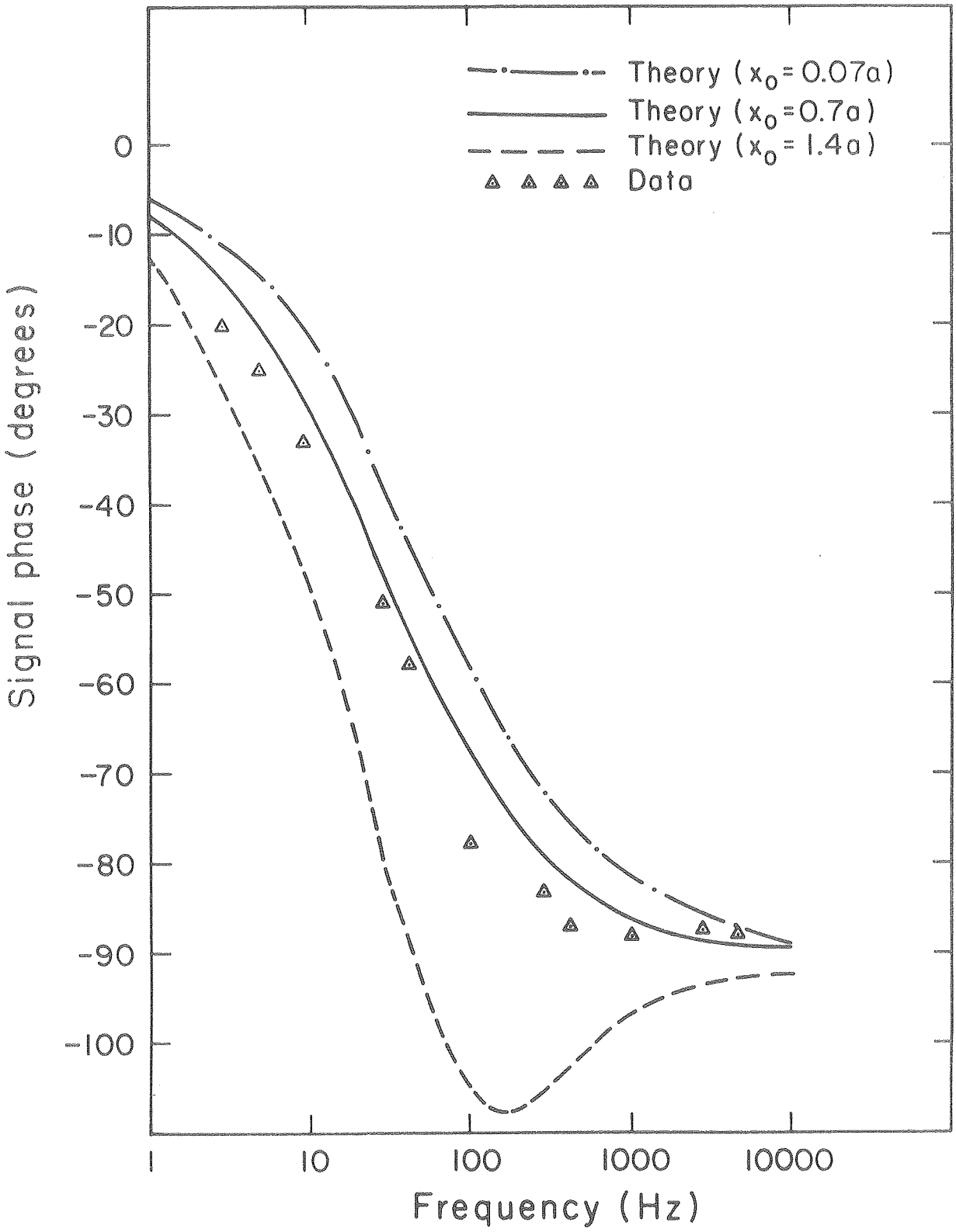

Fig. 7b XBL 8010-2077

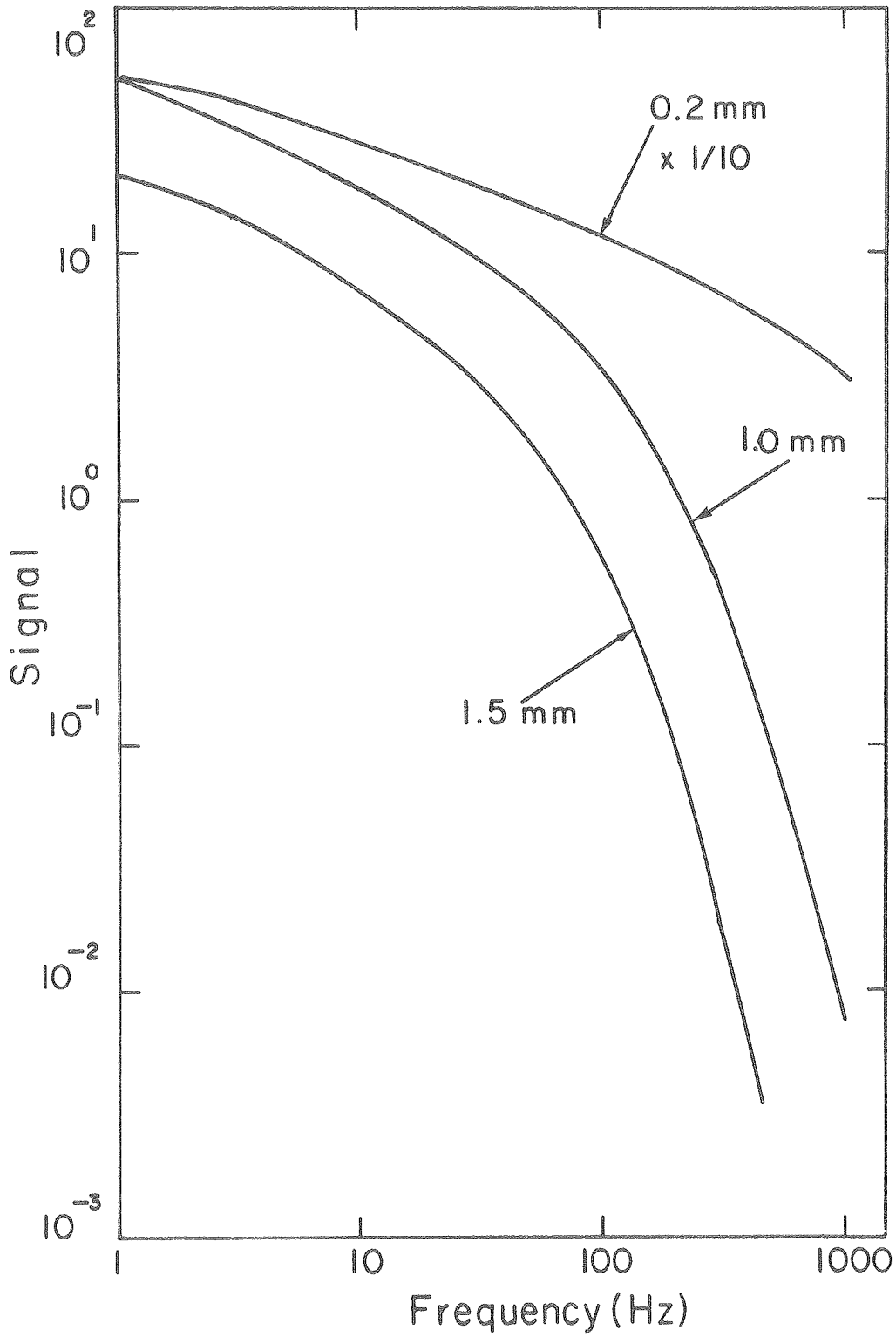

Fig. 8 XBL 8010-2074

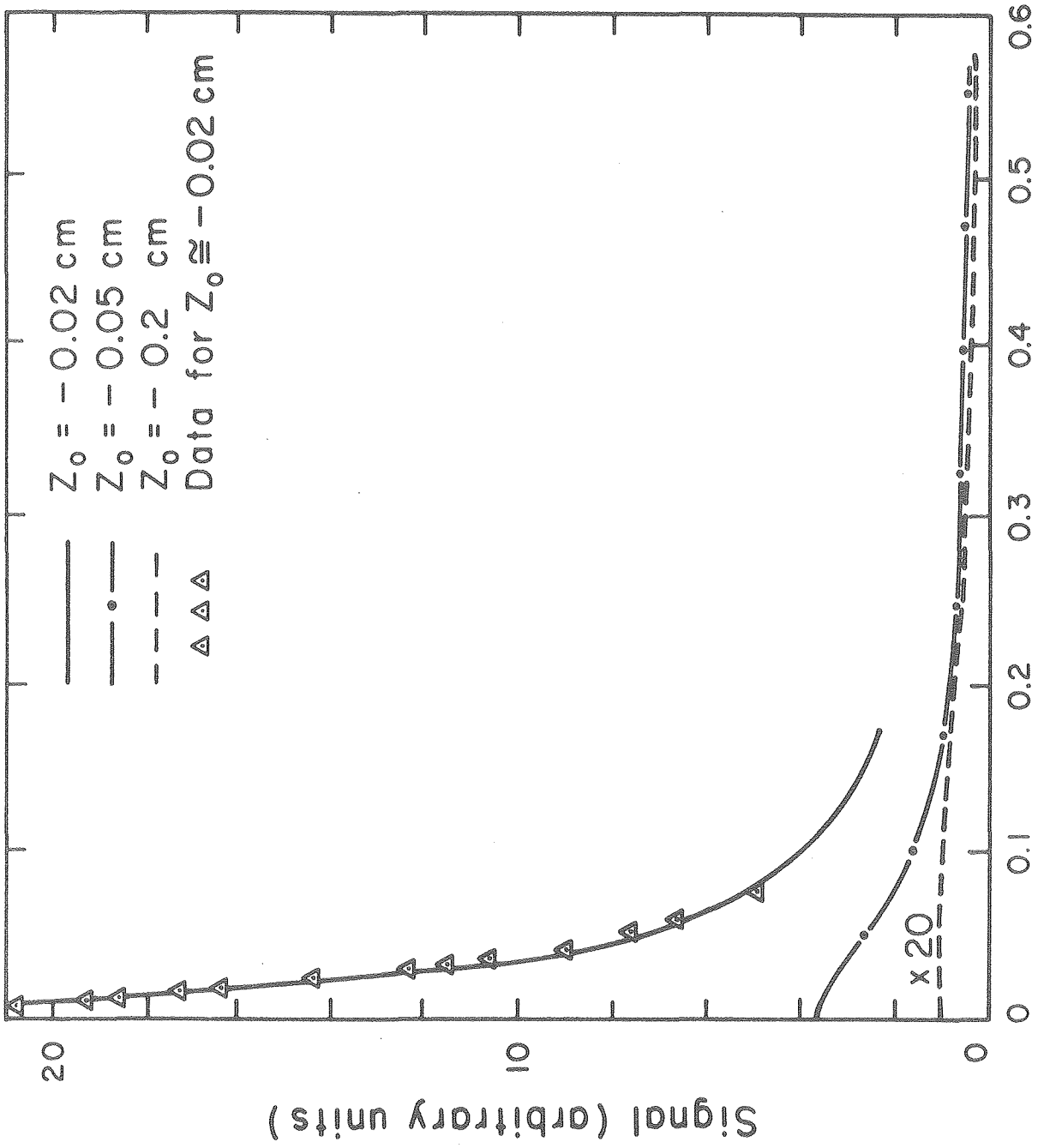

XBL 8010-2084

Fig. 9

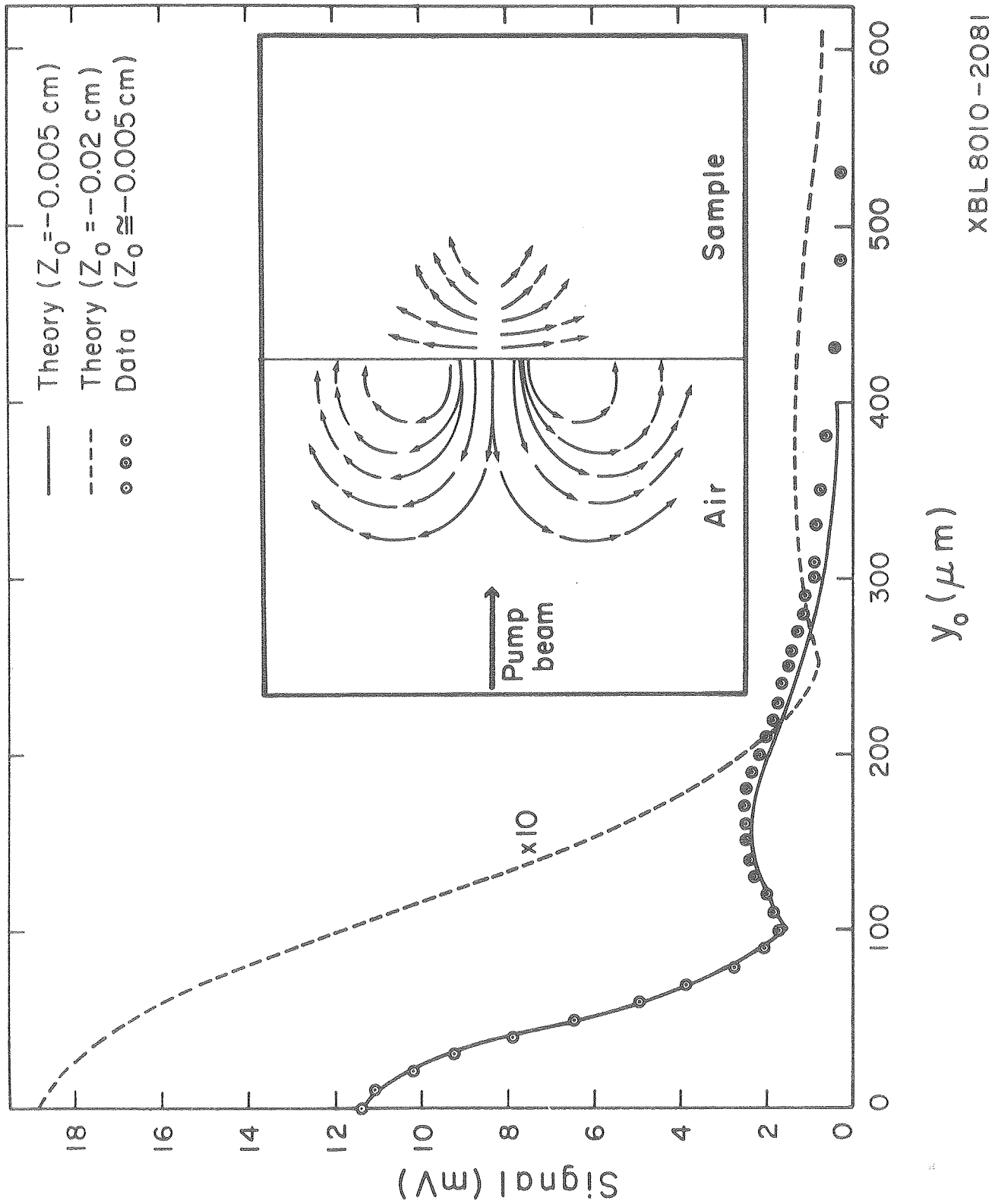

XBL 8010-2081

Fig. 10

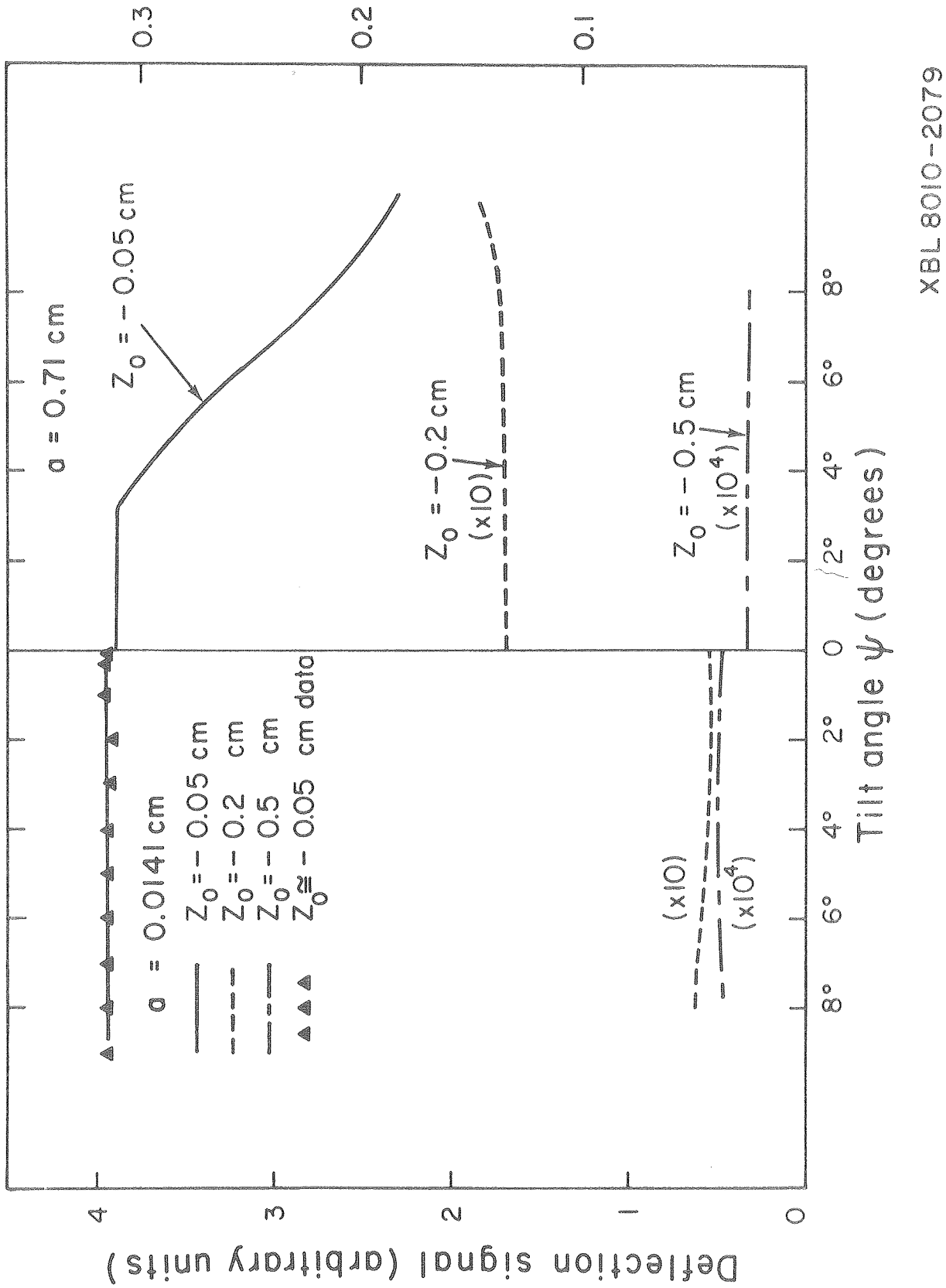
Deflection signal (arbitrary units)
Tilt angle ψ (degrees)
a = 0.71 cm
Z0 = − 0.05 cm
Z0 = −0.2 cm
(x10)
Z0 = − 0.5 cm
(x10⁴)
a = 0.0141 cm
Z0 = − 0.05 cm
Z0 = − 0.2 cm
Z0 = − 0.5 cm
Z0 ≅ − 0.05 cm data
XBL 8010-2079

Fig. 11

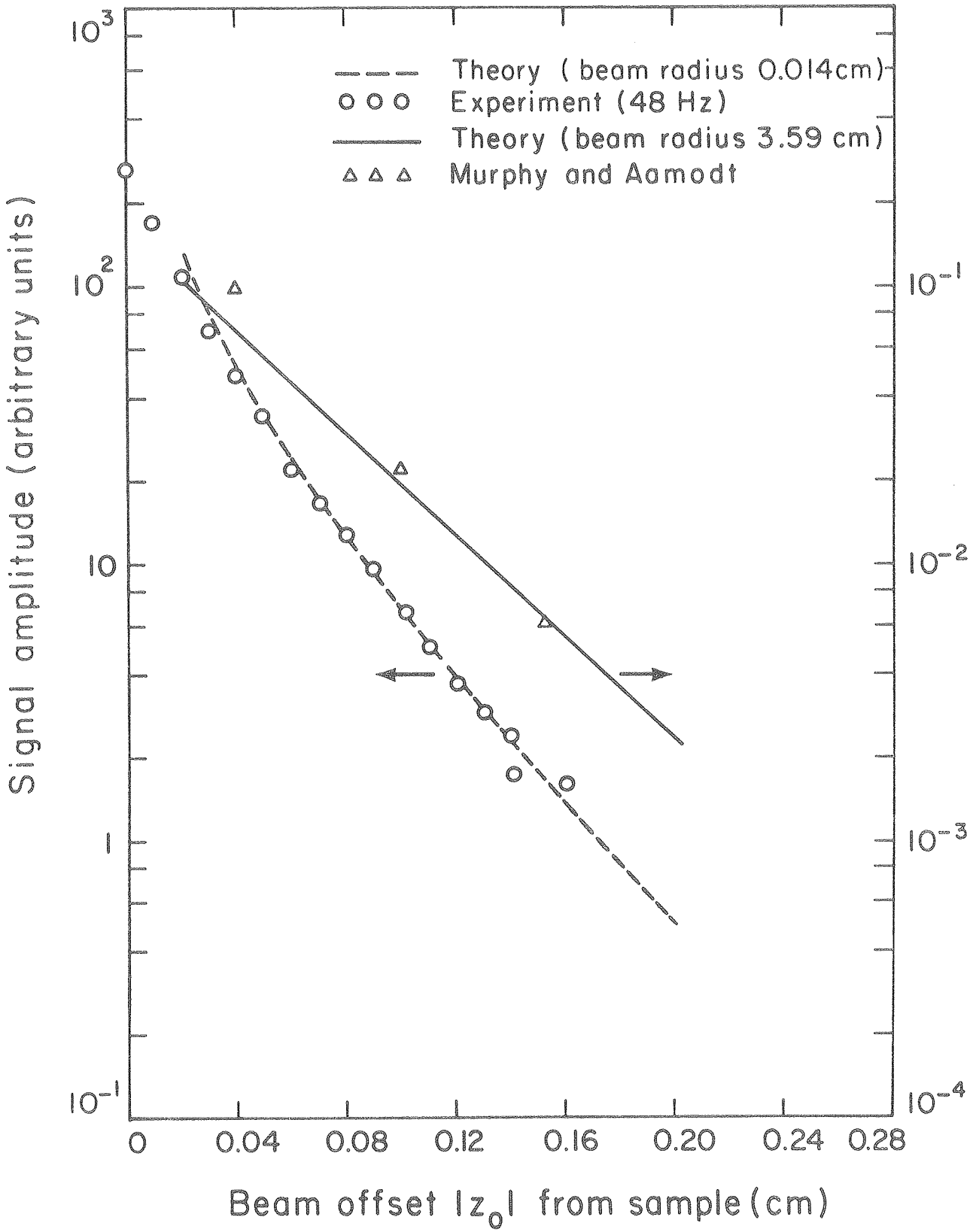

Fig. 12

XBL 8010-2076

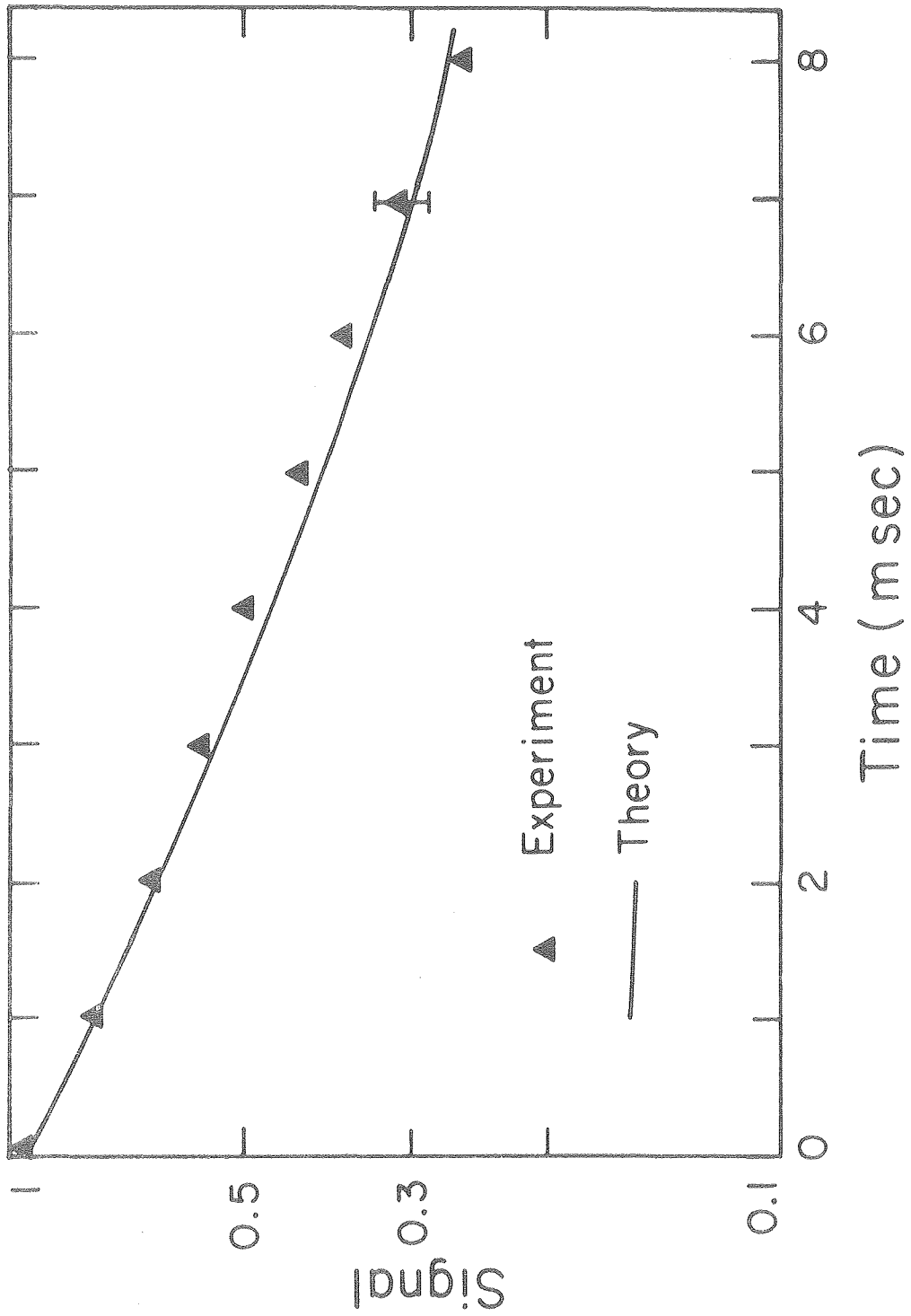
Signal
0.5
0.3
0.1
0
2
4
6
8
Time (msec)
Experiment
Theory
XBL 8010-2085

Fig. 13

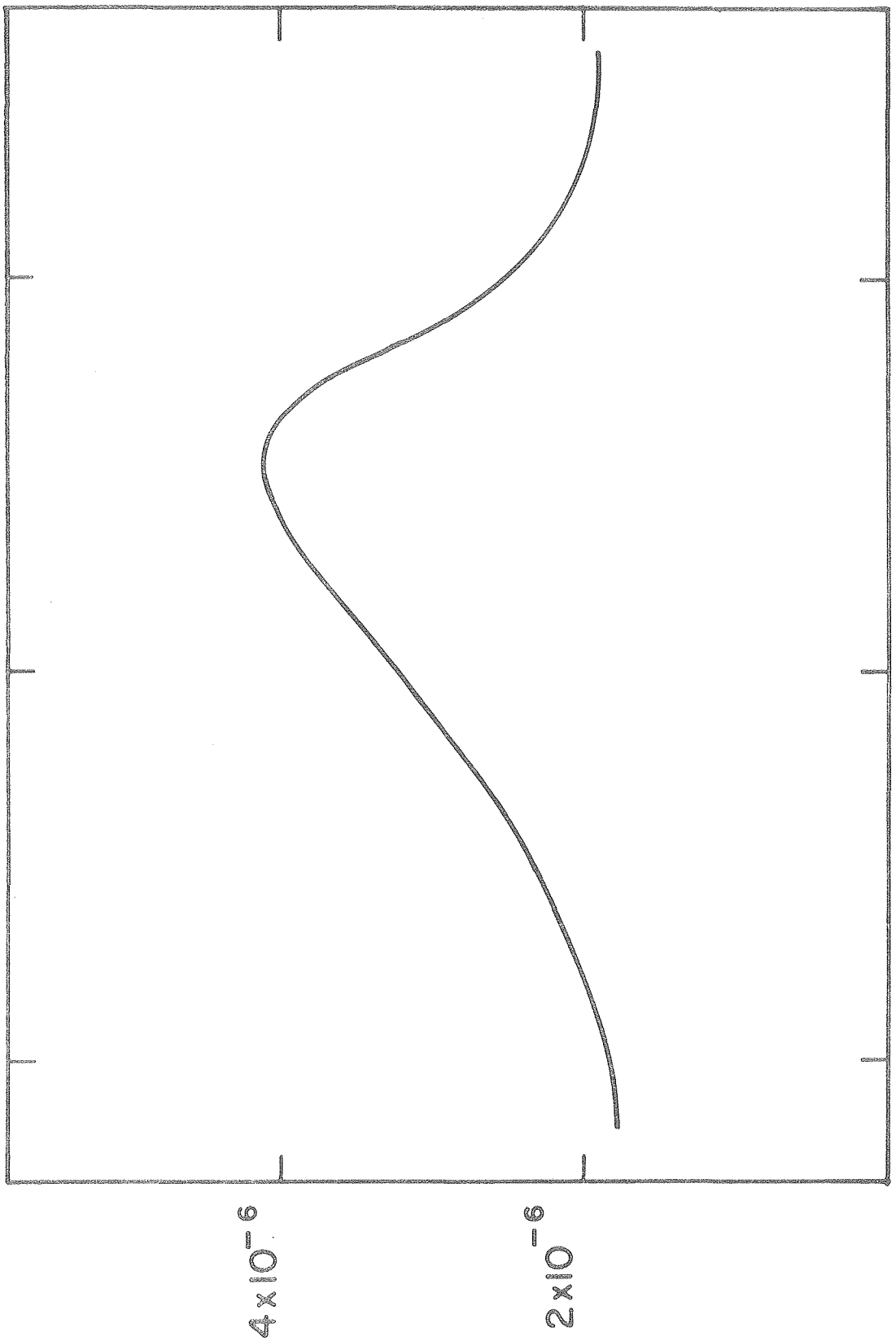

XBL8010-2086

Fig. 14a

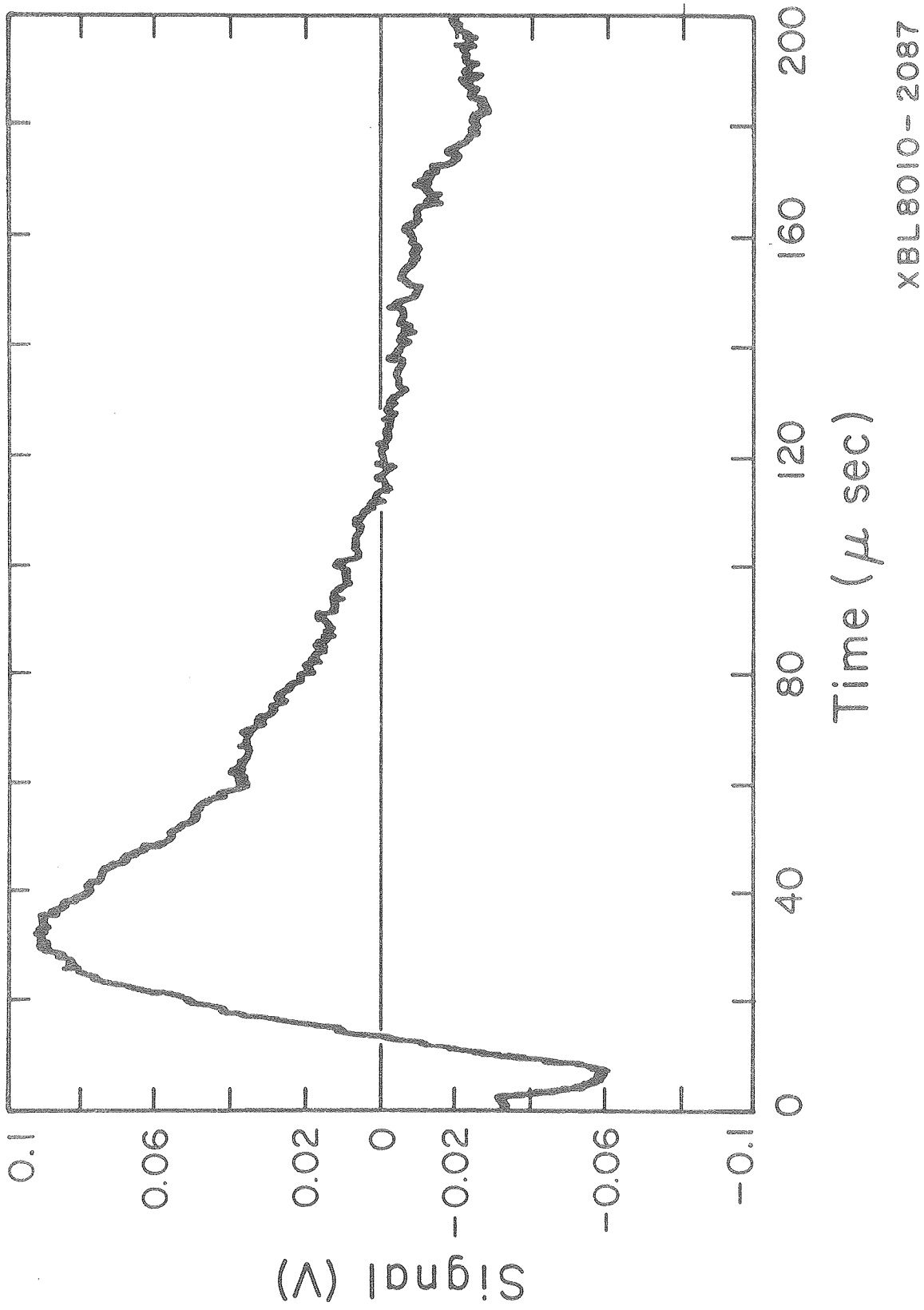
Signal (V)
0.1
0.06
0.02
0
-0.02
-0.06
-0.1
0
40
80
120
160
200
Time (μ sec)
XBL8010-2087

Fig. 14b